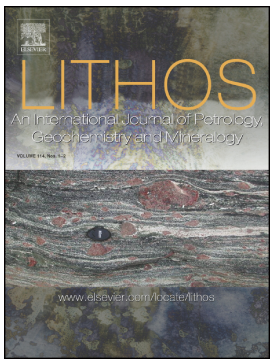

Petrogenetic and tectonic implications of major and trace element and radiogenic isotope geochemistry of Pliocene to Holocene rocks from the Tacaná Volcanic Complex and Chiapanecan Volcanic Belt, southern Mexico

Surendra P. Verma, Sanjeet K. Verma

PII: S0024-4937(18)30173-7
DOI: doi:10.1016/j.lithos.2018.05.016
Reference: LITHOS 4662

To appear in:

Received date: 18 December 2017
Accepted date: 13 May 2018

Please cite this article as: Surendra P. Verma, Sanjeet K. Verma , Petrogenetic and tectonic implications of major and trace element and radiogenic isotope geochemistry of Pliocene to Holocene rocks from the Tacaná Volcanic Complex and Chiapanecan Volcanic Belt, southern Mexico. The address for the corresponding author was captured as affiliation for all authors. Please check if appropriate. Lithos(2018), doi:10.1016/j.lithos.2018.05.016

Petrogenetic and tectonic implications of major and trace element and radiogenic isotope geochemistry of Pliocene to Holocene rocks from the Tacaná Volcanic Complex and Chiapanecan Volcanic Belt, southern Mexico

Surendra P. Verma[1,*], Sanjeet K. Verma[2]

[1] Instituto de Energías Renovables, Universidad Nacional Autónoma de México, Temixco, Mor. 62580, Mexico. spv@ier.unam.mx

[2] División de Geociencias, Instituto Potosino de Investigación en Ciencia y Tecnología, Camino a la Presa San José # 2055, Col. Lomas 4[a] Sec., San Luis Potosí, SLP 78216, Mexico. sanjeet.verma@ipicyt.edu.mx

Corresponding author, E-mail: spv@ier.unam.mx, phone +52-55-56229745

Manuscript submitted to: **Lithos**, December 18, 2017, revised April 4, 2018; Re-revised May 6, 2018.

Declarations of interest: none.

The authors have no competing interests.

A B S T R A C T

New major and trace element, and Sr, Nd and Pb isotope data for samples from the Volcán Tacaná, along with the published data from the Tacaná Volcanic Complex (TVC) and Chiapanecan Volcanic Belt (CVB), were used to better constrain the petrogenesis of the Pliocene to Holocene volcanism in southwestern Mexico. The TVC volcanic rocks sampled in this study were andesite, whereas the literature samples included, besides andesites, one subalkali basalt and a few dacites. The CVB housing the prominent El Chichón volcano, on the other hand, showed more alkalic magmatic products (trachyandesite and basaltic trachyandesite) but also included a few basalts and dacites. The enclaves and lithic fragments sampled from both TVC and CVB showed wide SiO_2 compositions similar to the volcanic products. The CVB rocks are more enriched in REE, LILE, and HFSE than the TVC. The combined data of volcanic rocks were evaluated through conventional multi-element diagrams as well as subduction- or crust-sensitive parameters. Although the TVC constitutes the northern end of the Central American Volcanic Arc (CAVA), some chemical differences were documented between them such as the TVC rocks have higher LILE, REE, HFSE, and combined ratio parameters. More importantly, the CVB seems to be significantly different from both TVC and CAVA as well as from other continental arcs such as higher LILE, REE, HFSE, and distinct isotopic signature, which may indicate that the origin of the CVB volcanism represents a direct action of the abundant strike-slip faults and extensional system prevalent in this area. Finally, the relationship of basic and evolved rocks from the CVB, especially on isotope-isotope diagrams, also suggests that the lower crust may have contributed to evolved magmas during the ascent of basic magmas through the crust.

Keywords

Central American Volcanic Arc, Tacaná Volcanic Complex, geochemometrics, southern Mexico, Chiapanecan Volcanic Arc, subduction, strike-slip faulting, extension

1. Introduction

The Quaternary Tacaná Volcanic Complex (TVC) constitutes mainly of the Tacaná, Chichuj, and San Antonio volcanoes, along with the Las Ardillas dome (García-Palomo et al., 2004; Mora et al., 2004; Macías et al., 2010; Arce et al., 2014). The Volcán Tacaná (~ 4,060 m high, meters above sea level), a stratovolcano, was active with phreatic explosions during 1986 (De la Cruz-Reyna et al., 1989; Mercado and Rose, 1992). The TVC, situated at the Mexico-Guatemala border, is shared by both countries (Fig. 1). It represents the northernmost part of the Central American Volcanic Arc (CAVA; Carr et al., 1990; Walker et al., 1995, 2000; Patino et al., 1997; Bolge et al., 2009). Geochemical studies of the Volcán Tacaná in particular and the TVC in general have been published by Macías et al. (2000, 2010), Mora et al. (2004, 2013), and Arce et al. (2014). All these authors documented detailed volcanological and geochronological studies for the TVC. However, although abundant major and trace element geochemical data were also reported by them, these data were not discussed in detail from the petrogenetic point of view.

The Pliocene to Holocene Chiapanecan Volcanic Belt (CVB; Fig. 1) of about 150 km long structure in the southwestern part of Mexico, is composed of at least six volcanoes as follows (Damon and Montesinos, 1978; Mora et al., 2007): Huitepec (0.85–1.95 Ma); Santa

Fe (2.17 Ma); Tzontehuitz (2.14–1.95 Ma); Zinacantan (0.85 Ma); Navenchauc (0.432 Ma); and El Chichón (situated at the northern end of the CVB is also considered a part of this province). The El Chichón volcano erupted violently in 1982, being the reason why this volcano has become the most studied volcano of the CVB.

Mora et al. (2007) reported geochemical data for a relatively large number of samples from several volcanic structures of the CVB (except the El Chichón volcano), but the discussion was mainly limited to the volcanological aspects of this area. Furthermore, these authors graphically showed differences between the CVB and CAVA for several trace element ratios, but commented little on their petrogenetic and tectonic implications.

For the well-studied El Chichón volcano, numerous tectonic, volcanologic, geochronologic, geochemical, and radiogenic isotope studies (Duffield et al., 1984; Rose et al., 1984; Rye et al., 1984; Tilling et al., 1984; Luhr et al., 1984; McGee et al., 1987; Espíndola et al., 2000; Tepley et al., 2000; Verma, 2002; De Ignacio et al., 2003; Macías et al., 2003; García-Palomo et al., 2004; Rosales Lagarde et al., 2006; Andrews et al., 2008; Manea and Manea, 2008; Layer et al., 2009; Carrera Muñoz, 2011; Arce et al., 2014; Scolamacchia and Macías, 2015) have been reported. In summary, Luhr et al. (1984) presented whole rock and mineral compositional data of the 1982 trachyandesite pumice and ash-fall eruptions of the El Chichón volcano and inferred that these andesites are more enriched in several elements than other andesites from Mexico and Central America. They also reported trace element partition coefficients for many minerals from the El Chichón volcano. Rye et al. (1984) reported sulfur and oxygen isotope systematics of the 1982 eruption of the El Chichón volcano and suggested that the data are consistent with either high-level assimilation of Cretaceous crustal evaporites or partial melting of volcanogenic

massive sulphides within the upper part of the subducted Cocos plate. Espíndola et al. (2000) presented radiocarbon ages and geochemical data of the El Chichón eruptions and concluded that at least 11 eruptions occurred during the last 8000 years, with repose periods of 100 to 600 years. De Ignacio et al. (2003) did not present any new data but, from some literature geochemical data, they hypothesized the presence of adakitic magmas among the eruptive products of the El Chichón volcano. Layer et al. (2009) presented geochemistry and $^{40}Ar/^{39}Ar$ ages from the El Chichón volcanic complex and highlighted the volcanic history of the El Chichón volcano during the past 0.37 Ma.

More recently, Arce et al. (2014) argued that the recently active Tacaná and El Chichón volcanoes represent a contrasting tectonic style. The Volcán Tacaná represents subduction-related volcanism, whereas the El Chichón volcano seems to have resulted from rift-dominated tectonics. However, the data presented by Mora et al. (2007) for other volcanoes of the CVB were not considered by Arce et al. (2014). Besides, the data from the Tacaná and El Chichón were only visually compared, without the application of any statistical tests.

The CVB is commonly called as the Chiapanecan Volcanic Arc (CVA; Damon and Montesinos, 1978; Luhr et al., 1984; Macías et al., 2003; García-Palomo et al., 2004; Mora et al., 2007; Andrews et al., 2008; Layer et al., 2009). If we could demonstrate from the application of appropriate statistical tests that the conclusion of Arce et al. (2014) is true for the entire CVB or CVA, the name of this volcanic province may have to be unified as the CVB, because then it will not be truly an arc (CVA). Therefore, an objective evaluation of all geochemical and isotopic data from both TVC and CVB is required, being the main goal of our study.

For radiogenic isotopes, only 6 samples from the TVC (4 eruptive products and 2 enclaves) were reported with Sr and Nd isotope data (Mora et al., 2004), and no Pb isotope data have yet been reported. Therefore, in addition to the geochemical data for the Volcán Tacaná, we report new Sr, Nd, and Pb isotopic data in this study. In order to better discuss the petrogenetic and tectonic implications, we compiled all available geochemical data from these two areas (TVC and CVB) and discussed them quantitatively along with the conventional multi-element normalization techniques. Statistically significant compositional differences have now been documented between these two volcanic areas (TVC and CVB) as well as from the CAVA, which seem to have resulted from differences in the regional tectonics, source characteristics, and petrogenetic processes.

2. Local geology of the study areas (TVC and CVB)

Macías et al. (2000, 2010) and Mora et al. (2004, 2013) have provided brief accounts of the local geology of the TVC representing the most northwesterly active volcanism of the CAVA. The TVC is located inside the NE-SW Tacaná graben and was built upon Mesozoic schists and gneisses intruded by Cenozoic granites, granodiorites and tonalities and covered by late Pliocene and early Pleistocene volcanic products (Mora et al., 2013). This region is characterized by a diffuse triple junction of Cocos–North American–Caribbean plates, delineated by the Middle America Trench (MAT) and Motagua-Polochic Fault (MPF) system (Fig. 1). Macías et al. (2000, 2010) suggested that the Tacaná volcano represents a part of the volcanic complex composed of three volcanic edifices (Chichuj, Tacaná, and San Antonio; Chj, TA, and SA, respectively, in Fig. 2) and the Las Ardillas dome (AD in Fig. 2). Macías et al. (2000, 2010) also reported ^{14}C ages, most of which are

Holocene. The TVC consists of four NE–SW aligned volcanic structures (Fig. 2) that are, from oldest to youngest, Chichuj (3800 m), Tacaná (4060 m), Las Ardillas Dome (3782 m), and San Antonio (3700 m). The locations of the samples analyzed in this study are shown schematically in Figure 2, which also includes the locations of the literature samples from the TVC.

The geology of the CVB, which is the least-studied volcanic province of Mexico in spite of the well-studied El Chichón volcano, has been presented by Mora et al. (2007). Briefly stated, the Pliocene to Holocene CVB rests on an older Paleocene to Pliocene igneous and sedimentary sequence, which in turn lies over Mesozoic and pre-Mesozoic metamorphic and sedimentary rocks. The oldest rocks (granites, diorites, and gneisses) are covered by sedimentary deposits and metamorphic rocks (serpentinites, schists, quarzites and gneisses), which are in turn intruded by gabbros, granodiorite, diorite and granite rocks of the Chiapas Batholith or Massif. The older igneous episode was in the Miocene and consisted of the intrusion of igneous rocks into the metamorphic rocks of the Chiapas Massif. The volcanic activity in the CVB during the Pliocene to Holocene was mainly effusive accompanied by some explosive and phreatomagmatic events and volcanic domes accompanied by block-and-ash-flows, ash flows with accretionary lapilli, falls, and pumice flows. The CVB region (Fig. 1) is characterized by both strike-slip and reverse faults (Guzmán-Speziale and Meneses-Rocha, 2000). The compression caused by the collision of the Yucatán block and Mexico in the Miocene (Kim et al., 2011) may have caused these reverse faults towards the right of the CVB area. From the locations of hypocenters associated with the faults, Guzmán-Speziale et al. (1989) proposed a wide and long zone of faults of lateral displacement with an extensional component as the continuation of the

Motagua-Polochic fault system (Fig. 1). Similar strike-slip faulting and extension and relationship of the CVB with them have been documented by Guzmán-Speziale and Meneses-Rocha (2000), Meneses-Rocha (2001) and Andreani et al. (2008).

3. Analytical methods and statistical procedures

Major and trace elements were determined by x-ray fluorescence spectrometry at the Johannes-Gutenberg Universität, Mainz, Germany. The analytical details and accuracy estimates were given by Verma et al. (1992). Radiogenic isotopes (Sr, Nd, and Pb) were analyzed on two fully-automated MAT 261 mass spectrometers at the Max Planck Institute, Mainz, Germany, following procedures summarized by Verma (1992).

All data were processed in the IgRoCS software (Verma and Rivera-Gómez, 2013) to automatically determine the magma and rock types under the Middlemost (1989) option for Fe-oxidation adjustment, which allowed us to strictly follow the IUGS recommendations for rock classification and nomenclature (Le Bas et al., 1986; Le Bas, 2000; Le Maitre et al., 1989, 2002). Thus, all major element data were treated in exactly the same manner. The use of 100% adjusted data on an anhydrous basis and after Fe-oxidation adjustment helps minimize the effect of analytical errors and element mobility and makes the use of the TAS diagram more consistent with the IUGS scheme. Petrogenetic interpretation was achieved through quantification of Nb and Ta anomalies in multi-element normalized diagrams, Sr-Nd-Pb radiogenic isotope systematics, and combined subduction- or crust-sensitive parameters.

The statistical (discordancy and significance) tests were applied to selected groups through UDASys2 software (Verma et al., 2016a, 2017a). The innovation in discordancy tests (Barnett and Lewis, 1994) consists in the recommended procedure which relies on the application of recursive tests (Rosner, 1975, 1977; Jain and Pingel, 1981; Verma et al., 2017b) at a strict 99% confidence level preceded by respective single-outlier tests (Grubbs, 1969; Grubbs and Beck, 1972) in order to achieve the best combination of high performance and low masking and swamping effects. Significance F and t tests were applied to the censored data provided by the recommended procedure of discordancy tests (Verma et al., 2016a, 2017a), which permitted us to identify statistically significant differences and similarities in two chosen groups of samples at a time (out of TVC, CVB, and CAVA). All tests were applied at the strict 99% confidence level to keep the type I error low at ~ 1%.

4. Results

4.1. Petrography of TVC and CVB

The TVC rocks show a porphyritic texture having lithics and enclaves, both of which consist of about 35 vol.% crystallinities for the Tacaná and Las Ardillas dome, and about 32 vol.% for the Chichuj volcano (Macías et al., 2000; Mora et al., 2004). Mafic enclaves exhibit an intersertal porphyritic texture, whereas lithic fragments show trachytic textures (Mora et al., 2004). The main minerals are plagioclase, hornblende, clinopyroxene, and orthopyroxene and all of them present disequilibrium features (Mora et al., 2004).

The CVB rocks show typical porphyritic and crystalline textures and have about 30 vol.% lithics and enclaves (Luhr et al., 1984). Both lithics and enclaves have a principal

mineral assemblage of plagioclase, amphibole, and clinopyroxene (Luhr et al., 1984; Arce et al., 2014). Anhydrite has been observed as a primary mineral in the El Chichón volcanic products (Luhr et al., 1984, Luhr, 1990). Epidote has also been documented as a hydrothermal mineral (Arce et al., 2014).

4.2. New analytical data

We present new major and trace element geochemical and Sr and Nd isotopic data for 11 Holocene samples and Pb isotope data for 5 selected samples from the Volcán Tacaná (Table 1). The results of processing of major element data of these samples in IgRoCS (Verma and Rivera-Gómez, 2013) as well as their online (https://tlaloc.ier.unam.mx) processing in HMgClaMSys (Verma et al., 2016b), MagClaMSys (Verma et al., 2017c) and IgRoClaMSys (Verma and Rivera-Gómez, 2017), were also included in Table 1. Although these recent multidimensional techniques are recommended for the nomenclature of altered igneous rocks (Verma et al., 2016b, 2017c; Verma and Rivera-Gómez, 2017), their use for fresh rocks and the consistency between the conventional (IUGS) and new (multidimensional) classification techniques provides a further test for the new online procedure. Consequently, this online procedure could be recommended for the classification and nomenclature of altered igneous rocks.

4.3. Literature data compilation

Besides the 11 samples from the Volcán Tacaná presented in this work, geochemical and isotopic data were compiled from both TVC (155 samples) and CVB (126 samples). The TVC literature references are as follows: Mercado and Rose (1992, 16 samples);

Macías et al. (2000, 8 samples); Mora et al. (2004, 59 samples); Macías et al. (2010, 13 samples); Limón Hernández (2011, 27 samples); Mora et al. (2013, 14 samples); and Arce et al. (2014, 18 samples).

The data for the CVB were compiled from the following sources: Luhr et al. (1984, 3 samples); Rose et al. (1984, 10 samples); McGee et al. (1987, 12 samples); Espíndola et al. (2000, 9 samples); Verma (2002; 1 sample); Macías et al. (2003, 8 samples); García-Palomo et al. (2004, 5 samples); Mora et al. (2007; 32 samples); Andrews et al. (2008, 7 samples); Layer et al. (2009, 8 samples); Carrera Muñoz (2011, 14 samples); and Arce et al. (2014, 17 samples).

Some unpublished material, such as Capaul (1987) cited in published papers, was not available to us, so those data could not be included in our database.

The compilation of data from the CAVA, other arcs, and continental rifts carried out by Verma (2015) was also used in this work.

4.4. Graphical representation of combined data

The new data from the TVC combined with the literature data from the TVC and CVB are presented in the conventional TAS diagram (Fig. 3a, b). Also included for comparison are the data from the CAVA compiled by Verma (2015), which cover a wide compositional range from basalt to rhyolite.

The volcanic rocks from the TVC are mainly andesite, with one basalt and a few samples of basaltic andesite and dacite (Fig. 3a), whereas those from the CVB are mainly trachyandesite and basaltic trachyandesite, but also include some samples of basalt, andesite, and dacite (Fig. 3b). One sample of granodiorite (Fig. 2 for location) was reported by Mora et al. (2004) and is used here as representing the upper crust of the TVC area; it

plotted in the rhyolite field (Fig. 3a). Lithic fragments and enclaves (described in the compiled papers) from both areas also show generally similar compositional variations (Fig. 3a, b). They are likely to be older than the volcanic products that brought them to the surface. The lithics and enclaves along with the granodiorite may represent compositions that may have modified the intermediate and acid magmas through crustal assimilation along with fractional crystallization (e.g., Rollinson, 1993). Nevertheless, it appears from the later presentation that the required probably lower crustal component has not yet been sampled and analyzed.

In alkali-enrichment, the TVC rocks (Fig. 3a) are generally similar to the CAVA, whereas the CVB rocks are more alkalic than CAVA (Fig. 3b). Note that the more alkalic rock varieties from the CAVA come from the back-arc locations (Verma, 2015). Unlike the limited rock types from the TVC and CVB, the CAVA rocks show a continuous variation from basalt to rhyolite (Fig. 3a, b).

Although the samples collected in this study were not analyzed for the rare earth elements (REE), REE data from both TVC and CVB were compiled from the literature. The chondrite-normalized diagrams are presented for the volcanic rocks of the TCV (Fig. 4a) and CVB (Fig. 4b), a granodiorite from the TVC area and lithic fragments and enclaves from both regions (Fig. 4c), and volcanic rocks from the CAVA (Fig. 4d). The average value of $(SiO_2)_{adj}$ is shown for reference for each magma type and the subsequent numbers refer to the total number of samples for calculating the average silica values. The total number of samples with the REE data for a given magma type is certainly less than these numbers. The chondrite-normalized La/Yb ratios $(La/Yb)_N$, along with the corresponding number of samples, are also included for each magma type (Fig. 4a-c). Because the number of samples for basic and acid volcanic rocks and enclaves from both TVC and CVB are

small and even lesser samples were analyzed for the REE (Fig. 4), we will comment on only the intermediate rocks.

The intermediate volcanic rocks from the TVC have lower REE concentrations (Fig. 4a) than the CVB rocks (Fig. 4b), but both areas (TVC and CVB) show higher concentrations than the CAVA (Fig. 4d). More importantly, the TVC intermediate rocks shows lower $(La/Yb)_N$ values (mean 7.6, n = 45, Fig. 4a; 99% confidence interval of the mean 7.3–8.0) than the CVB (mean 9.4, n = 50, Fig. 4b; 99% confidence interval of the mean 8.9–10.0). This inference is valid at the 99% confidence level. i.e., the TVC shows statistically lower REE enrichment (lower $(La/Yb)_N$ values) than the CVB. Both TVC and CVB depict higher $(La/Yb)_N$ values for intermediate rocks than the CAVA (mean 4.4, n = 310, Fig. 4d; 99% confidence interval of the mean 4.2–4.6). The intermediate lithics and enclaves from the TVC also show less REE enrichment and lower $(La/Yb)_N$ (mean 6.6, n = 14, Fig. 4c; 99% confidence interval of the mean 5.7–7.4) than the CVB area (mean 9.2, n = 8, Fig. 4c; 99% confidence interval of the mean 7.9–10.6). Therefore, it appears that the enrichment of the REE and $(La/Yb)_N$ is in the following sequence: CVB > TVC > CAVA.

For the CAVA, the mean REE concentrations, especially the light REE (La to Sm), increase in the sequence basic–intermediate–acid (Fig. 4d), which may support the dominant role of the fractional crystallization in their petrogenesis (for partition coefficients and modelling, see Rollinson, 1993; Verma, 1999; or Torres-Alvarado et al., 2003). For both TVC and CVB, on the other hand, such a progressive enrichment is not clear, which suggests that, crustal assimilation may have accompanied the fractional crystallization. Appropriate assimilants having lower concentrations of all incompatible elements, however, have not yet been sampled, although the granodiorite may provide characteristics suitable for the heavy REE (Fig. 4c).

Simplified multi-element primitive mantle-normalized diagrams are shown in Fig. 5. The TVC samples show (Fig. 5a) enrichment of large ion lithophile elements (LILE: Sr, K, Rb, and Ba) over the high field strength elements (HFSE: Nb, P, and Zr). However, such LILE enrichment with respect to the HFSE is much lower for the CVB volcanic rocks (Fig. 5b). A quantitative interpretation of such enrichment in these diagrams is provided in Section 5. The granodiorite sample included in Fig. 5a could provide appropriate assimilant for modelling of several elements, such as Nb (assuming Nb < 2 ppm detection limit reported by Mora et al., 2004), Zr, P, Ti, Y, and Yb, for the evolution of TVC intermediate and acid magmas (Rollinson, 1993; Torres-Alvarado et al., 2003).

Isotope-isotope diagrams are presented in Fig. 6. All Sr isotope data were adjusted to SRM987 $^{87}Sr/^{86}Sr$ of 0.710230 and Nd to La Jolla $^{143}Nd/^{144}Nd$ of 0.511860. Besides the present work (Table 1), the Sr and Nd isotope data for one acid and three intermediate volcanic rock samples from the TVC were taken from Mora et al. (2004). Unfortunately, the unique basaltic sample reported by Mora et al. (2004; sample no. 9702, their Table 3) for the TVC was not isotopically analyzed by them. Similarly, the only granodiorite sample (Mora et al., 2004; no. 9719) representing the upper continental crust beneath the TVC was also not analyzed for isotopes. Therefore, we do not have the information on basaltic magma and upper crust from the TVC area. On the other hand, from the CVB area, one sample of basaltic magma was reported by Espíndola et al. (2000; Sr and Nd isotopes) and one by Verma (2002; Sr, Nd, and Pb isotopes). Sr and Nd isotope data for intermediate volcanic rocks from the CVB were reported by Espíndola et al. (2000; 1 sample), Macías et al. (2003; 1 sample), and Andrews et al. (2008; 7 samples). The Pb isotope data from the CVB were reported by Andrews et al. (2008; 7 samples). García-Palomo et al. (2004), however, simply reproduced the isotope data of Espíndola et al. (2000). The relatively

similar values of Sr and Nd isotopes for three samples of lithic or enclave samples (two from the TVC by Mora et al., 2004; and one from the CVB by Macías et al., 2003) were not considered any further because they cannot provide appropriate crustal contaminant characteristics. Literature data for the CAVA, other arcs, and continental rifts as well as mantle components and lower crust are also included for reference in all diagrams (Fig. 6a-e).

On the conventional Sr-Nd isotope diagram (Fig. 6a), although the samples from both TVC and CVB plot within the mantle array, the TVC rocks seem to be shifted at higher $^{87}Sr/^{86}Sr$ values towards the "Downgoing slab" as compared to the CVB, but their $^{143}Nd/^{144}Nd$ values are similar and variable. The two basic rock samples from the CVB plot at higher $^{143}Nd/^{144}Nd$ but similar $^{87}Sr/^{86}Sr$ values as the evolved rocks. The CVB basic rocks also plot within the mantle array and suggest that at least two mantle components may be involved in the petrogenesis of this volcanic province but there seems to be no evidence of the subduction component (Fig. 6a). The CAVA rocks plot from the mantle array (Faure, 1986; Gopalan, 2017) to the trace of the "Downgoing slab", as is the case of all other arcs (Fig. 6a). The continental rift rocks plot mainly within and close to the mantle array. The relationship of basic and evolved rocks from the CVB may indicate assimilation of lower crustal material (indicated by LC from Rudnick and Fountain, 1995; Gopalan, 2017, in Fig. 6a) during the ascent of basic magmas through the crust.

On the $^{206}Pb/^{204}Pb$–$^{207}Pb/^{204}Pb$ diagram (Fig. 6b), the TVC rocks plot on the "Downgoing slab" line, whereas the CVB rocks plot between this and the NHRL (Northern Hemisphere Reference Line; Zindler and Hart, 1986). However, on this diagram (Fig. 6b), the distinction between the CAVA, other arcs and continental rifts is not clear. The relationship of basic and evolved magmas from the CVB may indicate a complex process

involving both assimilation and fractional crystallization. The indications from Fig. 6a of the involvement of lower crust can only be valid provided beneath the CVB the crust could have slightly higher $^{207}Pb/^{204}Pb$ than the location of LC in Fig. 6b. On the $^{206}Pb/^{204}Pb$–$^{208}Pb/^{204}Pb$ diagram (Fig. 6c), the downgoing slab and NHRL plot relatively close to each other. The TVC and CVB samples show lesser distinction than in Fig. 6b. Nevertheless, the relationship of basic and evolved magmas from the CVB (Fig. 6c) can be explained by the assimilation of lower crustal material as in Fig. 6a. Finally, the combined $^{206}Pb/^{204}Pb$–$^{87}Sr/^{86}Sr$ (Fig. 6d) and $^{206}Pb/^{204}Pb$–$^{143}Nd/^{144}Nd$ data (Fig. 6e) the TVC and CVB rocks show a clear distinction on both diagrams and the relationship of basic and evolved rocks from the CVB also indicates involvement of lower crust for their evolution. Note a mixing line can be drawn between the basalt and LC that passes through the intermediate rocks (Fig. 6d, e).

4.5. Statistical synthesis of combined data

First, we separated the samples from each area (TVC and CVB) into two groups: (1) volcanic products (133 samples from the TVC and 86 from the CVB); and (2) enclaves and lithic fragments (32 samples from the TVC and 26 from the CVB). Each group was then subdivided into three magma types (basic, intermediate, and acid). Only intermediate rocks had a sufficiently large number of samples worthy of further statistical analysis.

Synthesis of Nb- and Ta-anomalies (originally defined by Verma, 2009) for the TVC and CVB is given in Table 2 and compared with other tectonic areas. Tables 3 and 4 present the statistical information for the volcanic products and enclaves–lithic fragments, respectively, from the TVC and CVB. The variables include the following groups: major

elements, REE, other trace elements, and subduction- or crust-sensitive parameters proposed by Verma (2009, 2015). Also included in Table 3 is the statistical information for intermediate rocks from the CAVA. More information on these relatively newer compositional parameters is given in the following section.

4. Discussion

5.1. Nb- and Ta-anomalies

The multi-element normalized diagrams provide visual information on the relative behavior of chemical elements. Such information can be quantitatively used for a better interpretation of the data (Verma, 2009). In the primitive-mantle normalized diagram (Fig. 5a, b), the behavior of Nb (a HFSE) with respect to its neighbor elements Ba (a LILE) and La (a light rare-earth element−LREE) can be quantified from the following equation (Verma, 2015):

$$\left\{Nb/Nb^{*}\right\}_{pm} = \frac{2\cdot(Nb_{sa}/Nb_{pm})}{(Ba_{sa}/Ba_{pm})+(La_{sa}/La_{pm})}. \quad (1)$$

where the element symbols Nb, Ba, and La refer to the concentrations of these elements in a sample or normalizing material; the subscript $_{sa}$ stands for the sample and $_{pm}$ for the primitive mantle; the superscript * refers to the Nb concentration that would result from a smooth pattern for Ba to La on the primitive mantle-normalized multi-element diagram (Fig. 5). The parameter $\left\{Nb/Nb^{*}\right\}_{pm}$ is generally called as Nb-anomaly. Any other

normalization or calculation formula (such as geometric mean, instead of the simple mean) will only change the actual values, but not the conclusions. Ta-anomaly $\left\{Ta/Ta^{*}\right\}_{pm}$ can be similarly defined (Verma, 2015).

The Nb- and Ta-anomalies are more meaningful for discriminating different tectonic settings from basic and ultrabasic rocks (e.g., Verma, 2006, 2015), because such magmas are likely to have lesser crustal assimilation effects than the intermediate and acid rocks. The latter are likely to have more residence time in the crust as compared to basic magmas. The lesser crustal residence time is especially true for relatively "primitive" basic magmas having high MgO, Mg#, Ni, and Cr. The crustal contamination is likely to modify (increase) the size of these anomalies, generally making the $\left\{Nb/Nb^{*}\right\}_{pm}$ and $\left\{Ta/Ta^{*}\right\}_{pm}$ parameters smaller.

The statistical information of the Nb-anomaly for the intermediate rocks (Table 2; mean ± standard deviation of 0.124 ± 0.016; 99% confidence limits of the mean 0.107−0.140) and acid (0.112 ± 0.030; 0.083−0.142) from the TVC shows a large negative anomaly. The Ta-Anomaly for intermediate rocks from the TVC is similarly large (0.144 ± 0.045; 0.100−0.189; Table 2). The number of acid rock samples from both TVC and CVB is too small for the respective anomaly (Nb-anomaly for the CVB and Ta-anomaly for both areas) to be statistically meaningful; this is shown by "---" in Table 2. However, the sizes of the anomalies for the TVC are similar to the continental arcs, including the frontal part of the CAVA (Table 2). On the other hand, the intermediate rocks from the CVB show smaller negative Nb- and Ta-anomaly values for intermediate rocks (0.222 ± 0.023, 0.199−0.244; and 0.305 ± 0.024, 0.282−0.329, respectively). However, the intermediate

rocks are incapable of providing an unequivocal answer for tectonic setting (Table 2). We really need to sample and analyze basic rocks for this and other parameters to provide unambiguous inferences (Verma, 2006, 2009, 2015).

The effect of crustal contamination cannot be fully ruled out for evolved intermediate or acid magmas. To understand the mantle processes in any area, basic magmas in close equilibrium with the underlying mantle are the best candidates (Verma, 2015). Unfortunately, no such data are available for basic eruptive products from none of these two areas (Table 2). This makes it difficult to better constrain the petrogenetic processes in the underlying mantle, although radiogenic Sr, Nd, and Pb isotopic data have been of some help (Section 4.4).

5.2. Conventional major and trace element compositions

The compositional differences among basic magmas from the TVC, CVB, and CAVA could highlight the mantle source compositions and partial melting processes. Unfortunately, the scarcity of basic volcanic rocks from the TVC and CVB makes it difficult to infer these petrogenetic aspects. One volcanic rock sample of basaltic magma from the TVC (Mora et al., 2004) will not be of much help because of its evolved nature (very low MgO ~3.8%, Ni~14 μg/g, and Cr~16 μg/g contents). However, three basic rock samples from the CVB (Espíndola et al., 2000; Verma, 2002; Layer et al., 2009) could indicate mantle source characteristics because of their high MgO (~7.7–12.3%), Ni (~74–232 μg/g), Cr (~374–686 μg/g), and Mg# (59–72). Unfortunately, the number of analyses (n) is only 3 and not useful for statistical inferences, for which we have arbitrarily set the

lower limit as n > 5. Nevertheless, their isotopic characteristics were used for petrogenetic inferences (Section 4.4).

The composition of intermediate rocks, on the other hand, could probably indicate the magma evolution processes, such as fractional crystallization and crustal assimilation. However, we probably need to know the initial basic magma compositions from a relatively large number of samples, which are not available for the TVC and CVB. Nevertheless, it may still be worthwhile to apply statistical tests to intermediate magmas in order to infer similarities and differences among the three areas (TVC, CVB, and CAVA). Some indications about the ratio parameters for the initial magma may be obtained from this exercise.

The synthesis presented in Table 3 shows that the intermediate rocks from the TVC, CVB, and CAVA show progressively lower SiO_2 concentrations (for simplicity, we are not reproducing henceforth the subscript "adj" in the text). Significance *t*-test confirmed that these differences are statistically significant at 99% confidence level. Hence forth, to highlight the similarities and differences among the three groups (TVC, CVB, and CAVA), we will base our discussion on the results of the significance tests (F and t), without mentioning this every time. However, we will report only those cases with n > 5 for each of the three groups under comparison.

The intermediate rocks from the TVC showed significantly higher concentrations (at > 99% confidence level) than the CVB for the following 8 elements (Table 3): SiO_2, MgO, Co, Hf, Pb, Sb, Sc, and Zn. For all other elements (the remaining 8 major elements, all 8 REE, and 12 trace elements listed in Table 3), the TVC showed significantly lower concentrations than the CVB, except Cr and Ni, for which no significant difference was

observed. The higher concentrations of all 8 REE (La to Lu), alkalis (Na_2O and K_2O), LILE (Rb, Cs, Ba, Sr), HFSE (Nb, Ta, Zr, P) as well as some ratio parameters (see Section 5.3) at a lower SiO_2 concentration level for the CVB as compared to the TVC (Table 3) may indicate similar enrichment in the CVB initial basic magmas that evolved to give rise to the intermediate magmas.

Concerning the TVC and CAVA, the following 18 elements showed statistically higher concentrations (Table 3) for the TVC: SiO_2, Na_2O, K_2O, La, Ce, Nd, Sm, Yb, Ba, Cs, Hf, Nb, Pb, Rb, Sb, Th, U, and Zr. Four elements (TiO_2, Tb, Lu, and Ta) did not show any significant differences between the TVC and CAVA. The intermediate rocks from the TVC for the remaining 16 elements have lower concentrations than the CAVA (Table 3).

Finally, the statistical comparison of intermediate rocks from the CVB with the CAVA indicated that the former rocks are higher in concentration than the latter for the following 31 elements (25 shown in Table 3): SiO_2, MnO, Na_2O, K_2O, P_2O_5, all 14 REE (shown only 8 in Table 3), Ba, Cs, Hf, Nb, Pb, Rb, Sr, Th, U, Y, and Zr. Three elements (TiO_2, Sb, and V) showed no significant differences, whereas the remaining 10 elements showed lower concentrations for the CVB than the CAVA (Table 3). These differences in intermediate magmas may also indicate similar differences between the respective basic magmas from the CVB and CAVA.

The lithic fragments and enclaves from the TVC show significantly lower concentrations of the following 17 elements as compared to the CVB (Table 4): SiO_2, Na_2O, K_2O, P_2O_5, La, Ce, Nd, Sm, Eu, Cs, Nb, Rb, Sr, Th, U, Y, and Zr. Similarly, the following 5 elements showed higher concentrations for the TVC than the CVB: TiO_2,

$Fe_2O_3^t$, MgO, Cr, and Zn (Table 4). The remaining 14 elements listed in Table 4 showed no significant differences between the TVC and CVB.

5.3. Subduction- or continental crust-sensitive parameters

Several combined subduction signal parameters were proposed to identify the subduction contribution in a tectonic environment (Verma, 2009, 2015). Higher values of such parameters, especially those having LILE in the numerator and HFSE in the denominator, likely reflect contribution from the subduction process. Alternatively or concurrently, high values of these parameters may also represent a significantly higher influence from the continental crust. This is especially true for evolved intermediate and acid rocks. Unfortunately, these considerations make it difficult to unambiguously infer the tectonic implications from evolved rocks. Nevertheless, we used 8 such parameters (one listed below; others in the Supplementary file) for statistically comparing the TVC, CVB, and CAVA.

The $(LILE4/LREE3)_E$ parameter is the "four LILE to three LREE" ratio (i.e. the ratio of averaged behavior of K, Rb, Ba, and Sr to the averaged behavior of La, Ce, and Nd) as follows:

$$\{\text{LILE4/LREE 3}\}_E = \frac{\left[(K_{sa}/K_E)+(Rb_{sa}/Rb_E)+(Ba_{sa}/Ba_E)+(Sr_{sa}/Sr_E)\right]/4}{\left[(La_{sa}/La_E)+(Ce_{sa}/Ce_E)+(Nd_{sa}/Nd_E)\right]/3} \qquad (2)$$

where the subscript "sa" stands for the sample and "E" for bulk silicate earth (normalization values taken from McDonough and Sun, 1995). Other parameters ($(LILE5/HFSE5a)_E$, $(LILE4/HFSE4a)_E$, $(LILE4/HFSE4b)_E$, $(LILE4/HFSE4c)_E$, $(LILE4/HFSE3a)_E$,

$(LREE3/HFSE5a)_E$; and $(LREE3/HFSE4a)_E$; equations 3-9) are listed in the Supplementary file.

The TVC intermediate rocks show higher values for 7 out of 8 parameters than the CVB (Table 3); the exception is the LREE3/HFSE4a, which is slightly lower for the TVC than the CVB. The intermediate rocks from the TVC also show higher values for 6 out of 8 parameters than the CAVA (Table 3); for the last two parameters in Table 3 the TVC rocks show lower values. These differences imply that the TVC rocks might represent a greater contribution from the crust than the CAVA. As compared to the CAVA, the intermediate rocks from the CVB show higher values for 1 parameter (LILE4/HFSE3a), no difference for 3 parameters (LILE5/HFSE5a, LILE4/HFSE4a, and LREE3/HFSE4a), and lower values for the remaining 4 parameters (Table 3). These differences are either due to differences in the contribution of the continental crust or may also represent differences in the tectonic regimes of the three areas (TVC, CVB, and CAVA).

Finally, out of the 5 parameters listed in Table 4, the intermediate lithic fragments and enclaves from the TCV show higher values for 1 parameter (LILE4/LREE3), lower values for 1 parameter (LREE3/HFSE4a), and no difference for the remaining 3 parameters. These similarities and differences simply show the characteristics of the upper crust represented by these lithics and fragments.

5.4. Multidimensional tectonic discrimination diagrams

The tectonics of southern Mexico is quite complex (Fig. 1). There is a diffuse triple junction near the TVC, which constitutes the northern end of the CAVA. The Cocos plate is being subducted beneath both the North American and Caribbean plates, with the division

being featured by the Tehuantepec Ridge (TeR; Fig. 1) on the oceanic plate and the Motagua-Polochic fault system on-land (MPF; Fig. 1). In the CVB area, there are abundant strike-slip and other extensional faults as well as the presence of compression represented by reverse faults (Fig. 1; see also Guzmán-Speziale and Meneses-Rocha, 2000; Meneses-Rocha, 2001). Besides, there is evidence of the collision of the Yucatan block with southern Mexico during the Miocene (Kim et al., 2011) and of the formation of the Southern Mexico Block (SMB; Fig. 1) in its initial stage as a separate identity from the North American plate (Andreani et al., 2008). In complex tectonic settings, for example, in western Mexico with ongoing subduction of the Rivera plate and the formation of a triple-rift system, hybrid tectonic answers are obtained from multidimensional discrimination (Verma et al., 2016c).

For the above reasons, multidimensional discrimination is not likely to provide any unequivocal or unique answer for the tectonic setting. Besides, the near absence of basic magmas from our combined database did not allow us to apply multidimensional diagrams for basic magmas. The diagrams for intermediate magmas provided inferences of hybrid tectonic settings for both TVC and CVB (the results are not presented in a tabular form). Therefore, we did not include these indications in the present paper.

5.5. Geophysical constraints

Seismic studies have indicated that the subducted Cocos plate can only be traced back to shallow depths beneath Mexico, whereas beneath Central America, its geometry is a standard textbook case, reaching depths of around 100 to 200 km beneath the CAVA (Fig. 1; Burbach et al., 1984; Guzmán-Speziale and Meneses-Rocha, 2000). The Motagua-Polochic fault system, the triple junction, and abundant strike-slip and other extensional

faults in southern Mexico (Fig. 1) may have caused the differences in subduction of the oceanic plate beneath the North American and Caribbean plates. Thus, even close to the CVB area of Mexico, the Cocos plate is still very shallow (subhorizontal) and may have reached only about 50 km depth (e.g., Guzmán-Speziale and Meneses-Rocha, 2000). Kim et al. (2011) proposed that approximately beneath the CVB, the Yucatan block collided in the Miocene with southern Mexico and broke the subducted Cocos plate.

Andreani et al. (2008) stated as follows (reproduced textually): "Numerous studies, mainly based on structural and paleomagnetic data, consider southern Mexico as a crustal block (southern Mexico block, SMB) uncoupled from the North American plate with a southeast motion with respect to North America, accommodated by extension through the central Trans-Mexican volcanic belt (TMVB)." Campos-Enríquez et al. (2015) inferred from gravity and seismic studies that the central part of the MVB (Fig. 1) may be subject to NW-SE to N-S extension with minor E-W left-lateral movement. Verma et al. (2016d) recently published new occurrences of extension-related magma close to the volcanic front of the central MVB and provided additional information on this complex modern plate tectonic problem. Yet another volcanic province in southern Mexico (LTVF; Fig. 1) was also interpreted as an extension-related volcanic field, in which the basic and ultrabasic magmas originated from a garnet-bearing mantle source (Verma. 2006). Verma (2002) documented that, in the whole of southern Mexico, there are no basic magmas related to the subduction of the Cocos plate. Arce et al. (2014; and references therein) documented abundant extensional or rift structures beneath the study area of CVB. All these studies may allow us to propose that there may be a new plate at the very initial stage of formation (Fig. 1; see also the SMB in Andreani et al., 2008), which may also render that the subducted

Cocos plate does not pass away beneath the CVB, as envisioned by Verma (2015) for the MVB. Verma (2015) outlined a model, according to which mantle upwelling taking place beneath the MVB will have to be accompanied by downwelling (mantle upward flow has to be compensated from a down flow), either at the north or south of the MVB, or both. The down flow in the south of the MVB may render the Cocos subducted plate to become aseismic beneath about 60 km depth away from the MVB. In the light of the documented extension and rift-structures beneath the CVB, we may extend this model (Verma, 2015) to whole of southern Mexico.

The model proposed by Manea and Manea (2008) is based on assumptions of deeper subducted slab unsupported by direct seismic evidence. Its deep presence relies on extrapolations (Pardo and Suárez, 1995) unsupported from more recent seismic observations (e.g., Pacheco and Singh, 2010). A shallow (around 50 km depth) slab beneath the CVB is unlikely to generate magma from the subduction process of the Tehuantepec Ridge. Likewise, the "flat" subduction envisioned by Manea et al. (2013) will be incapable of providing mechanism for causing the generation of magmas due to the shallow nature of the subducted slab. Diminished volcanism and different arc-unlike characteristics have been documented in the Andes associated with "flat-slab" (e.g., Kay et al., 1991).

More constraints, especially the study of basic volcanic rocks and underlying crust from both areas and appropriate well-constrained thermochemical models, are required before a comprehensive petrogenetic and tectonic model could be put forth. This should be part of a future study.

Conclusions

The volcanic products from the TVC and CVB are mainly of intermediate compositions. The basic and acid rocks are relatively scarce, but there is an urgent need to sample and analyze basic rocks from both areas to better understand the mantle processes. The TVC rocks showed large Nb and Ta anomalies similar to the CAVA and other arcs, whereas the CVB showed somewhat smaller anomalies. The intermediate rocks from the TVC showed significant differences from the CVB (higher concentrations for 8 elements, lower for 28 elements, and no difference for only 2 elements). The TVC showed higher concentrations that the CAVA for 18 elements, lower for 16 elements, and no difference for only 4 elements. Between the CVB and CAVA, the CVB volcanic rocks showed higher concentrations for 25 elements, lower for 10 elements, and no difference for only 3 elements. Similarly, the lithic fragments and enclaves from the TVC and CVB showed for the TVC intermediate rocks, higher concentrations for 5 elements, lower for 17 elements, and no differences for 14 elements. In terms of subduction- or crust-sensitive parameters, the TVC, CVB, and CAVA showed significant differences in several parameters. These differences may highlight the characteristics of the underlying mantle or more likely, the continental crust. Finally, it appears that the Chiapenecan Volcanic Belt (CVB) could be the unified name of this volcanic province because it may not be truly an arc (CVA could therefore be abandoned).

Acknowledgements

This work was partly supported by IER-UNAM internal grant to the first author. SKV is grateful to Newton Advance Fellowship award–The Royal Society, UK for the grant

[NA160116]. We are grateful to Venancio de la Cruz Martínez and Marcos Milán for providing the Volcán Tacaná samples and their petrographic description. We thank Servando de la Cruz-Reyna for having provided us a copy of the paper by Rose et al. (1984). The manuscript was written and finalized during a sabbatical stay of the first author at the IPICYT. We are also grateful to two anonymous reviewers for constructive comments on an earlier version of our manuscript and Prof. Nelson Eby for its editorial handling.

References

Andreani, L., Le Pichon, X., Rangin, C., Martínez-Reyes, J., 2008. The southern Mexico block: main boundaries and new estimation for its Quaternary motion. Bulletin de la Societe géologique de France 179 (2), 209–223.

Andrews, B.G., Gardner, J.E., Housh, T.B., 2008. Repeated recharge, assimilation, and hybridization in magmas erupted from El Chichón as recorded by plagioclase and amphibole phenocrysts. Journal of Volcanology and Geothermal Research 175, 415–426.

Arce, J.L., Walker, J., Keppie, J.D., 2014. Petrology of two contrasting Mexican volcanoes, the Chiapanecan (El Chichón) and Central American (Tacaná) volcanic belts: the result of riftversus subduction-related volcanism. International Geology Review 56 (4), 501–524.

Barnett, V., Lewis, T., 1994. Outliers in statistical data. John Wiley & Sons, Chichester, 584 pp.

Bolge, L.L., Carr, M.J., Milidakis, K.I., Lindsay, F.N., Feigenson, M.D., 2009. Correlating geochemistry, tectonics, and volcanic volume along the Central American Volcanic front. Geochemistry, Geophysics, Geosystems 10, 15.

Burbach, G.V., Frohlich, C., Pennington, W.D., Matumoto, T., 1984. Seismicity and tectonics of the subducted Cocos plate. Journal of Geophysical Research 89 (B9), 7719–7735.

Campos-Enríquez, J.O., Lermo-Samaniego, J.F., Antayhua-Vera, Y.T., Chavacán, M., Ramón-Márquez, V.M., 2015. The Aztlán Fault System: control on the emplacement of the Chichinautzin Range volcanism, southern Mexico basin, Mexico, seismic and gravity characterization. Boletín de la Sociedad Geológica Mexicana 67 (2), 315–335.

Capaul, W.A., 1987. Volcanoes of the Chiapas Volcanic Belt, Mexico. Ph.D. Thesis, Michigan Technological University, Michigan, U.S.A., 93 pp.

Carr, M.J., Feigenson, M.D., Bennett, E.A., 1990. Incompatible element and isotopic evidence for tectonic control of source mixing and melt extraction along the Central American arc. Contributions to Mineralogy and Petrology 105 (4), 369–380.

Carrera Muñoz, M., 2011. Geoquímica y petrología del Arco Volcánico Chiapaneco (AVC) porción norte, Chiapas, México. Master´s Thesis, Universidad Nacional Autónoma de México, Mexico, D.F., 112 pp.

Damon, P., Montesinos, E., 1978. Late Cenozoic volcanism and metallogenesis over an active Benioff Zone in Chiapas, Mexico. Arizona Geological Society Digest 11, 155–168.

De Ignacio, C., Castiñeiras, P., Márquez, A., Oyarzun, R., Lillo, J., López, I., 2003. El Chichón volcano (Chiapas Volcanic Belt, Mexico) transitional calc-alkaline to adakitic-like magmatism: petrologic and tectonic implications. International Geology Review 45, 1020–1028.

De la Cruz-Reyna, S., Armienta, M.A., Zamora, V., Juárez, F., 1989. Chemical changes in spring waters at Tacaná volcano, Chiapas, Mexico: a possible precursor of the May 1986 seismic crisis and phreatic explosion. Journal of Volcanology and Geothermal Research 38, 345–353.

Duffield, W.A., Tilling, R.I., Canul, R., 1984. Geology of El Chichón volcano, Chiapas, Mexico. Journal of Volcanology and Geothermal Research 20, 117–132.

Espíndola, J.M., Macías, J.L., Tilling, R.I., Sheridan, M.F., 2000. Volcanic history of El Chichón volcano (Chiapas, Mexico) during the Holocene, and its impact on human activity. Bulletin of Volcanology 62, 90–104.

Faure, G., 1986. Principles of isotope geology. Second edition, Wiley, New York, 653 pp.

García-Palomo, A., Macías, J.L., Espíndola, J.M., 2004. Strike-slip faults and K-alkaline volcanism at el Chichón volcano, southeastern Mexico. Journal of Volcanology and Geothermal Research 136, 247–268.

Gopalan, K., 2017. Principles of radiometric dating. Cambridge University Press, Cambridge, 207 pp.

Grubbs, F.E., 1969. Procedures for detecting outlying observations in samples. Technometrics 11 (1), 1–21.

Grubbs, F.E., Beck, G., 1972. Extension of sample sizes and percentage points for significance tests of outlying observations. Technometrics 14 (4), 847–854.

Guzmán-Speziale, M., Meneses-Rocha, 2000. The North America–Caribbean plate boundary west of the Motagua–Polochic fault system: a fault jog in Southeastern Mexico. Journal of South American Earth Sciences 13, 459–468.

Guzmán-Speziale, M., Pennington, W.D., Matumoto, D., 1989. The triple junction of North American, Cocos and Caribbean plates: Seismicity and tectonics. Tectonics 8, 981–997.

Jain, R.B., Pingel, L.A., 1981. On the robustness of recursive outlier detection procedures to nonnormality. Communications in Statistics - Theory and Methods 10 (13), 1323–1334.

Kay, S.M., Mpodozis, C., Ramos, V.A., Munizaga, F., 1991. Magma source variations for mid-late Tertiary magmatic rocks associated with a shallowing subduction zone and a thickening crust in the central Andes. Geological Society of America Special Paper 265, 113–137.

Kim, W.H., Clayton, R.W., Keppie, F., 2011. Evidence of a collision between the Yucatán block and Mexico in the Miocene. Geophysical Journal International 187 (2), 989–1000.

Layer, P.W., García-Palomo, A., Jones, D., Macías, J.L., Arce, J.L., Mora, J.C., 2009. El Chichón volcanic complex, Chiapas, México: stages of evolution based on field mapping and $^{40}Ar/^{39}Ar$ geochronology. Geofísica Internacional 48 (1), 33–54.

Le Bas, M.J., 2000. IUGS reclassification of the high-Mg and picritic volcanic rocks. Journal of Petrology 41 (10), 1467–1470.

Le Bas, M.J., Le Maitre, R.W., Streckeisen, A., Zanettin, B., 1986. A chemical classification of volcanic rocks based on the total alkali-silica diagram. Journal of Petrology 27 (3), 745–750.

Le Maitre, R.W., Streckeisen, A., Zanettin, B., Le Bas, M.J., Bonin, B., Bateman, P., Bellieni, G., Dudek, A., Schmid, R., Sorensen, H., Woolley, A.R., 1989. A classification of igneous rocks and glossary of terms: recommendations of the International Union of Geological Sciences Subcommission of the Systematics of igneous rocks. Blackwell Scientific Publications, Oxford, 193 pp.

Le Maitre, R.W., Streckeisen, A., Zanettin, B., Le Bas, M.J., Bonin, B., Bateman, P., Bellieni, G., Dudek, A., Schmid, R., Sorensen, H., Woolley, A.R., 2002. Igneous rocks. A classification and glossary of terms: recommendations of the International Union of Geological Sciences Subcommission of the Systematics of Igneous Rocks. Cambridge University Press, Cambridge, 236 pp.

Limón Hernández, C.G., 2011. Estratigrafía y morfología de los flujos de lava y depósitos asociados a la actividad efusiva del Volcán Tacaná, México-Guatemala. Master´s Thesis, Universidad Nacional Autónoma de México, México, D.F., 125 pp.

Luhr, J.F., 1990. Experimental phase relations of water- and sulfur-saturated arc magmas and the 1982 eruptions of El Chichón volcano. Journal of Petrology 31, 1071–1114.

Luhr, J.F., Carmichael, I.S.E., Varekamp, J.C., 1984. The 1982 eruptions of El Chichón volcano, Chiapas, Mexico: mineralogy and petrology of the anhydrite-bearing pumices. Journal of Volcanology and Geothermal Research 23, 69–108.

Macías, J.L., Espíndola, J.M., García-Palomo, A., Scott, K.M., Hughes, S., Mora, J.C., 2000. Late Holocene Peléan-style eruption at Tacaná volcano, Mexico and Guatemala: past, present, and future hazards. Geological Society of America Bulletin 112, 1234–1249.

Macías, J.L., Arce, J.L., Mora, J.C., Espíndola, J.M., Saucedo, R., Manetti, P., 2003. A 550-year-old Plinian eruption at El Chichón volcano, Chiapas, Mexico: explosive volcanism linked to reheating of the magma reservoir. Journal of Geophysical Research 108 (B12), 2569, doi:10.1029/2003JB002551.

Macías, J.L., Arce, J.L., García-Palomo, A., Mora, J.C., Layer, P.W., Espíndola, J.M., 2010. Late-Pleistocene flank collapse triggered by dome growth at Tacaná volcano, México-Guatemala, and its relationship to the regional stress regime. Bulletin of Volcanology 72, 33–53.

Manea, M., Manea, V.C., 2008. On the origin of El Chichón volcano and subduction of Tehuantepec Ridge: A geodynamical perspective. Journal of Volcanology and Geothermal Research 175, 459–471.

Manea, V.C., Manea, M., Ferrari, L. 2013. A geodynamical perspective on the subduction of Cocos and Rivera plates beneath Mexico and Central America. Tectonophysics 609, 56–81.

McDonough, W.F., Sun, S.-s., 1995. The composition of the Earth. Chemical Geology 120, 223–253.

McGee, J.J., Tilling, R.I., Duffield, W.A., 1987. Petrologic characteristics of the 1982 and pre-1982 eruptive products of el Chichon volcano, Chiapas, Mexico. Geofísica Internacional 26, 85–108.

Meneses-Rocha, J.J., 2001. Tectonic evolution of the Ixtapa graben, an example of a strike-slip basin in southeastern Mexico: Implications for regional petroleum systems, in Bartolini, C. Buffler, R.T., and Cantú-Chapa, A. (eds.), The western Gulf of Mexico Basin: Tectonics, sedimentary basins, and petroleum systems: American Association of Petroleum Geologists Memoir 75, 183–216.

Mercado, R, Rose, W.I., 1992. Reconocimiento geológico y evaluación preliminar de peligrosidad del volcán Tacaná, Guatemala/México. Geofísica Internacional 31 (3), 205–237.

Middlemost, E.A.K., 1989. Iron oxidation ratios, norms and the classification of volcanic rocks. Chemical Geology 77 (1), 19–26.

Mora, J.C., Macías, J.L., García-Palomo, A., Arce, J.L., Espíndola, J.M., Manetti, P., Vaselli, O., Sánchez, J.M., 2004. Petrology and geochemistry of the Tacaná Volcanic complex, Mexico-Guatemala: evidence for the last 40 000 yr of activity. Geofísica Internacional 43(3), 331–359.

Mora, J.C., Jaimes-Viera, M.C., Garduño-Monroy, V.H., Layer, P.W., Pompa-Mera, V., Godinez, M.L., 2007. Geology and geochemistry characteristics of the Chiapanecan

Volcanic Arc (Central Area), Chiapas Mexico. Journal of Volcanology and Geothermal Research 162, 43–72.

Mora, J.C., Gardner, J.E., Macías, J.L., Meriggi, L., Santo, A.P., 2013. Magmatic controls on eruption dynamics of the 1950 yr B.P. eruption of San Antonio Volcano, Tacaná Volcanic Complex, Mexico-Guatemala. Journal of Volcanology and Geothermal Research 262, 134–152.

Pacheco, J.F., Singh, S.K., 2010. Seismicity and state of stress in Guerrero segment of the Mexican subduction zone. Journal of Geophysical Research 115 (B01303), doi:10.1029/2009JB006453.

Pardo, M., Suárez, G., 1995. Shape of the subducted Rivera and Cocos plates in southern Mexico: Seismic and tectonic implications. Journal of Geophysical Research 100 (B7), 12,357–12,373.

Patino, L.C., Carr, M.J., Feigenson, M.D., 1997. Cross-arc geochemical variations in volcanic fields in Honduras C.A.: progressive changes in source with distance from the volcanic front. Contributions to Mineralogy and Petrology 129 (4), 341–351.

Reagan, M.K., Gill, J.B., 1989. Coexisting calcalkaline and high-niobium basalts from Turrialba volcano, Costa Rica: implications for residual titanates in arc magma sources. Journal of Geophysical Research 94, 4619–4633.

Rollinson, H.R., 1993. Using geochemical data: evaluation, presentation, interpretation. Longman Scientific Technical, Essex, 344 pp.

Rosales Lagarde, L., Boston, P.J., Campbell, A., Stafford, K.W., 2006. Possible structural connection between Chichón volcano and the sulfur-rich springs of Villa Luz Cave (a.k.a. Cueva de las Sardinas), Southern Mexico. AMCS Bulletin 19, 177–184.

Rose Jr., W.I., Bornhorst, T.J., Halsor, S.P., Capaul, W.A., Plumley, P.S., De la Cruz-Reyna, S., Mena, M., Mota, R., 1984. Volcán El Chichón, Mexico: Pre-1982 S-rich eruptive activity. Journal of Volcanology and Geothermal Research 23 (1-2), 147–149.

Rosner, B., 1975. On the detection of many outliers. Technometrics 17 (2), 221–227.

Rosner, B., 1977. Percentage points for the RST many outlier procedure. Technometrics 19 (3), 307–312.

Rotolo, S.G., Castorina, F., 1998. Transition from midly-tholeiitic to calc-alkaline suite: the case of Chicontepec volcanic centre, El Salvador, Central America. Journal of Volcanology and Geothermal Research 86, 117–136.

Rudnick, R.L., Fountain, D.M., 1995. Nature and composition of the continental crust: a lower crustal perspective. Reviews of Geophysics 33 (3) 267–309.

Ryder, C.H., Gill, J.B., Tepley III, F., Ramos, F., Reagan, M., 2006. Closed- to open-system differentiation at Arenal volcano (1968-2003). Journal of Volcanology and Geothermal Research 157, 75–93.

Rye, R.O., Luhr, J.F., Wasserman, M.D., 1984. Sulfur and oxygen isotopic systematics of the 1982 eruptions of El Chichón volcano, Chiapas, Mexico. Journal of Volcanology and Geothermal Research 23, 109–123.

Scolamacchia, T., Macías, J.L. (Eds.), 2015. Active volcanoes of Chiapas (Mexico): El Chichón and Tacaná. Active Volcanoes of the World, Springer-Verlag, Berlin, 180 p.

Singer, B.S., Smith, K.E., Jicha, B.R., Beard, B.L., Johnson, C.M., Rogers, N.W., 2011. Tracking open-system differentiation during growth of Santa María volcano, Guatemala. Journal of Petrology 52 (12), 2335–2363.

Sun, S.-S., McDonough, W.F., 1989. Chemical and isotopic systematics of oceanic basalts: implications for mantle composition and processes. In: A.D. Saunders and M.J. Norry (Editors), Magmatism in the ocean basins. Geological Society Special Publication, 313–345.

Tepley, F.J.I., Davidson, J.P., Tilling, R.I., Arth, J.G., 2000. Magma mixing, recharge and eruption histories recorded in plagioclase phenocrysts from El Chichón volcano, Mexico. Journal of Petrology 41 (9), 1397–1411.

Tilling, R.I., Rubin, M., Sigurdsson, H., Carey, S., Duffield, W.A., Rose, W.I., 1984. Holocene eruptive activity of El Chichón volcano, Chiapas, México. Science 224, 747–749.

Torres-Alvarado, I.S., Verma, S.P., Palacios-Berruete, H., Guevara, M., González-Castillo, O.Y., 2003. DC_Base: a database system to manage Nernst distribution coefficients and its application to partial melting modeling. Computers & Geosciences 29 (9), 1191–1198.

Verma, S.P., 1992. Seawater alteration effects on REE, K, Rb, Cs, Sr, U, Th, Pb, and Sr-Nd-Pb isotope systematics of mid-ocean ridge basalt. Geochemical Journal 26 (3), 159–177.

Verma, S.P., 1999. Geochemistry of evolved magmas and their relationship to subduction-unrelated mafic volcanism at the volcanic front of the central Mexican Volcanic Belt. Journal of Volcanology and Geothermal Research 93 (1–2), 151–171.

Verma, S.P., 2000. Geochemistry of the subducting Cocos plate and the origin of subduction-unrelated mafic volcanism at the volcanic front of the central Mexican Volcanic Belt, in Delgado-Granados, H., Aguirre-Díaz, G. and Stock, J.M. (eds.), Cenozic Tectonics and Volcanism of Mexico, Boulder, Colorado: Geological Society of America,. Special Paper 334, 195–222.

Verma, S.P., 2002. Absence of Cocos plate subduction-related basic volcanism in southern Mexico: a unique case on Earth? Geology 30 (12), 1095–1098.

Verma, S.P., 2006. Extension-related origin of magmas from a garnet-bearing source in the Los Tuxtlas volcanic field, Mexico. International Journal of Earth Sciences 95 (5), 871–901.

Verma, S.P., 2009. Continental rift setting for the central part of the Mexican Volcanic Belt: a statistical approach. Open Geology Journal 3, 8–129.

Verma, S.P., 2015. Present state of knowledge and new geochemical constraints on the central part of the Mexican Volcanic Belt and comparison with the Central American

Volcanic Arc in terms of near and far trench magmas. Turkish Journal of Earth Sciences 24 (5), 399–1460.

Verma, S.P., Rivera-Gómez, M.A., 2013. Computer programs for the classification and nomenclature of igneous rocks. Episodes 36 (2), 115–124.

Verma, S.P, Rivera-Gómez, M.A., 2017. Transformed major element based multidimensional classification of altered volcanic rocks. Episodes 40 (4), 295–303.

Verma, S.P., Besch, T., Guevara, M., Schulz-Dobrich, B., 1992. Determination of twelve trace elements in twenty-seven and ten major elements in twenty-three geochemical reference samples by X-Ray fluorescence spectrometry. Geostandards Newsletter 16 (2), 301–309.

Verma, S.P., Díaz-González, L., Pérez-Garza, J.A., Rosales-Rivera, M., 2016a. Quality control in geochemistry from a comparison of four central tendency and five dispersion estimators and example of a geochemical reference material. Arabian Journal of Geosciences 9 (20), 740.

Verma, S.P., Rivera-Gómez, M.A., Díaz-González, L., Quiroz-Ruiz, A., 2016b. Log-ratio transformed major-element based multidimensional classification for altered High-Mg igneous rocks. Geochemistry Geophysics Geosystems 17 (12), 4955–4972.

Verma, S.P., Pandarinath, K., Rivera-Gómez, M.A., 2016c. Evaluation of the ongoing rifting and subduction processes in the geochemistry of magmas from the western part of the Mexican Volcanic Belt. Journal of South American Earth Sciences 66, 125–148.

Verma, S.P., Torres-Sánchez, D., Velasco-Tapia, F., Subramanyam, K.S.V., Manikyamba, C., Bhutani, R., 2016d. Geochemistry and petrogenesis of extension-related magmas close to the volcanic front of the central part of the Trans-Mexican Volcanic Belt. Journal of South American Earth Sciences 72, 126–136.

Verma, S.P., Díaz-González, L., Pérez-Garza, J.A. and Rosales-Rivera, M., 2017a. Erratum to: Quality control in geochemistry from a comparison of four central tendency and five dispersion estimators and example of a geochemical reference material. Arabian Journal of Geosciences 10 (2), 24.

Verma, S.P., Rosales-Rivera, M., Díaz-González, L., Quiroz-Ruiz, A., 2017b. Improved composition of Hawaiian basalt BHVO-1 from the application of two new and three conventional recursive discordancy tests. Turkish Journal of Earth Sciences 26 (5), 331-353.

Verma, S.P., Rivera-Gómez, M.A., Díaz-González, L., Pandarinath, K., Amezcua-Valdez, A., Rosales-Rivera, M., Verma, S.K., Quiroz-Ruiz, A., Armstrong-Altrin, J.A., 2017c. Multidimensional classification of magma types for altered igneous rocks and application to their tectonomagmatic discrimination and igneous provenance of siliciclastic sediments. Lithos 278, 321–330.

Walker, J.A., Carr, M.J., Patino, L.C., Johnson, C.M., Feigenson, M.D., Ward, R.L., 1995. Abrupt change in magma generation processes across the Central America arc in southeastern Guatemala: flux-dominated melting near the base of the wedge to decompression melting near the top of the wedge. Contributions to Mineralogy and Petrology 120, 378–390.

Walker, J.A., Patino, L.C., Cameron, B.I., Carr, M.J., 2000. Petrogenetic insights provided by compositional transects across the Central American arc: southeastern Guatemala and Honduras. Journal of Geophysical Research 105 (B8), 18949–18963.

Zindler, A., Hart, S., 1986. Chemical geodynamics. Annual Review of Earth and Planetary Science 14, 493–571.

Figure legends

Fig.1. Location map of the study area in southern Mexico (modified after Verma, 2002; Guzmán-Espeziale and Meneses-Rocha, 2000; Meneses-Rocha, 2001; and Andreani et al., 2008); southern Mexico and Central America are subjected to the complex interaction of five tectonic plates (Cocos, Pacific, Rivera, North American, and Caribbean; besides the Southern Mexico Block at the initial stage of separation from the North American plate). The abbreviations are as follows: TVC – Tacaná Volcanic Complex; CVB – Chiapanecan Volcanic Belt; CAVA—Central American Volcanic Arc; LTVF—Los Tuxtlas Volcanic Field; SMB—Southern Mexico Block; MVB—Mexican Volcanic Belt; MAT—Middle American Trench; EPR—East Pacific Rise; TeR—Tehuantepec Ridge; CoR—Cocos Ridge; MPF—Motagua-Polochic fault; and G—Guatemala. The volcanoes of the CVB (Huitepec, Santa Fe, Tzontehuitz, Zinacantan, and Navenchauc) cannot be distinguished properly on this map scale, except the El Chichón volcano situated at the northern end of the CVB. The numbers on dotted lines on-land give approximate depths (in km) of the subducting Cocos slab (see the deepest contour of about 60 km beneath southern Mexico, with no deeper earthquakes beneath the CVB, whereas the 200 km deep contour seems to lie close to the CAVA). The two curvilinear trends from the Pacific coast to mainland Mexico (one towards the MVB and the other towards the LTVF) show schematically the dense seismic network used by the UNAM–CalTech collaborative project to better locate the subducted Cocos slab beneath Mexico (e.g., Pacheco and Singh, 2010; Kim et al., 2011).

Fig. 2. Schematic sample location map of the Tacaná Volcanic Complex (TVC), modified after an unpublished map by Venancio de la Cruz Martínez. The abbreviations are as follows: TA–Tacaná; Chj—Chichuj; SA—San Antonio; and AD—Las Ardillas dome. The compiled samples (volcanic rocks, lithics, and enclaves) from the literature are from Mercado and Rose (1992), Macías et al. (2000, 2010), Mora et al. (2004, 2013), Limón-Hernández (2011), and Arce et al. (2014); the granodiorite sample representing "TVC upper crust" from the lower right corner of the map was collected and analyzed by Mora et al. (2004; sample 9719).

Fig. 3. Conventional TAS (total alkalis Na_2O+K_2O versus silica SiO_2; Le Bas et al., 1986; both axes in mass/mass units expressed in percent, %m/m, adjusted adj. composition from Verma and Rivera-Gómez, 2013) diagram for the samples analyzed in this study and compiled from the literature (see text for details). The classification fields are as follows: PB—picrobasalt; B—basalt; BA—basaltic andesite; A—andesite; D—dacite; R—rhyolite; TB—trachybasalt; BTA—basaltic trachyandesite; TA—trachyandesite; TD—trachydacite; BSN—basanite; and TEP—tephrite; and PHT—phonotephrite. Other abbreviations are as follows: TVC—Tacaná Volcanic Complex; CVB—Chiapanecan Volcanic Belt; and CAVA—Central American Volcanic Arc. The symbols to distinguish rock samples from the TVC and CVB are shown as insets; CAVA samples for comparison are reproduced in each diagram. a) TVC along with CAVA; b) CVB along with CAVA.

Fig. 4. Chondrite-normalized rare-earth element (REE) diagrams for the TCV, CVB, and CAVA rocks (chondrite values for normalization taken from the compilation of McDonough and Sun, 1995; the mean silica $(SiO_2)_{adj}$ values along with the number of samples as well as the mean chondrite-normalized La/Yb ratios $(la/Yb)_N$ along with the respective number of samples are also included for each rock type). (**a**) basic to acid volcanic rocks from the TVC; (**b**) basic to acid volcanic rocks from the CVB; (**c**) mean compositions of basic to acid enclaves and lithic fragments from the TCV and CVB as well a granodiorite representing upper crust beneath the TVC area (the uncertainties in REE normalized values–not shown–show overlaps, only the mean values for the CVB are higher than for the CVB); and (**d**) basic to acid volcanic rocks from the CAVA.

Fig. 5. Primitive-mantle normalized multi-element diagrams for eruptive products (see text for details on literature references) from (**a**) Tacaná Volcanic Complex (TVC), also included is a sample from the upper crust; (**b**) Chiapanecan Volcanic Belt (CVB). Primitive mantle values for normalization were taken from Sun and McDonough (1989).

Fig. 6. Conventional isotope-isotope diagrams for the Tacaná Volcanic Complex (TVC; 11 samples from this work; 4 samples from Mora et al., 2004) and Chiapanecan Volcanic Belt (CVB; 7 samples Andrews et al., 2008; 3 samples Espíndola et al., 2000; 1 sample Macías et al., 2003; 1 sample Verma, 2002); less samples were analyzed for Pb; The symbols are shown as insets in (a); trace of the "Downgoing slab" is from Verma (2000) and the numbers of this curve indicate the amount of sediment (%) in the altered MORB-sediment

mixture; mantle components (BSE–bulk silicate earth, DM–DMM–depleted mantle, EM1–enriched mantle type-I component, EM2–enriched mantle type-II component, HM–HIMU–high-μ, and PM–PREMA–prevalent mantle) and NHRL (Northern Hemisphere Reference Line) are from Zindler and Hart (1986); see also Gopalan (2017); LC–highly heterogeneous lower crust (mean value is indicated in diagrams) from Rudnick and Fountain (1995) and Gopalan (2017); several components lie outside the diagrams, which is indicated by arrows pointing towards the approximate direction in which they are located; Central American Volcanic Arc (CAVA) from Reagan and Gill (1989), Carr et al. (1990), Walker et al. (1995, 2000), Patino et al. (1997), Rotolo and Castorina (1998), Ryder et al. (2006), and Singer et al. (2011); data from other arcs (Aleutians, Fiji, Lesser Antilles, Mariana, Papua New Guinea, Philippines, and Sunda-Banda) and continental rifts (Abu Gabra, China (E, N, NE, SE), East Africa, Ethiopia, Turkey (Kula), Basin and Range, Colorado Plateau, Rio-Grande, and Utah) compiled by Verma (2015) are also included; (**a**) $^{87}Sr/^{86}Sr$—$^{143}Nd/^{144}Nd$, for comparison, schematic trace of the mantle array (Faure, 1986; Gopalan, 2017); (**b**) $^{206}Pb/^{204}Pb$—$^{207}Pb/^{204}Pb$; (**c**) $^{206}Pb/^{204}Pb$—$^{208}Pb/^{204}Pb$; (**d**) $^{206}Pb/^{204}Pb$—$^{87}Sr/^{86}Sr$; and (**e**) $^{206}Pb/^{204}Pb$—$^{143}Nd/^{144}Nd$.

Table 1

New geochemical data (major oxides and CIPW norm in %m/m and trace elements in μg/g) of the Quaternary volcanic rock samples from the Volcán Tacaná; Mexico-Guatemala border.

Sample:	VTA01	VTA03	VTA04	VTA08	VTA11	VTA12	VTA18	VTA19	VTA27	VTA29	VTA37
Petrographic type: *	Hornblende andesite	Hornblende andesite	Hornblende andesite	Hornblende augite andesite	Hornblende andesite	Augite andesite	Augite andesite	Augite hornblende andesite	Hornblende andesite	Augite andesite	Andesite
Magma−type: **	Intermediate	Intermediate	Intermediate	Intermediate	Intermediate	Intermediate	Intermediate	Intermediate	Intermediate	Intermediate	Intermediate
Rock−type (IUGS): **	Andesite	Andesite	Andesite	Andesite	Andesite	Andesite	Andesite	Andesite	Andesite	Andesite	Andesite
HMgClaMSys ***	Common igneous rock	Common igneous rock	Common igneous rock	Common igneous rock	Common igneous rock	Common igneous rock	Common igneous rock	Common igneous rock	Common igneous rock	Common igneous rock	Common igneous rock
MagClaMSys ***	Intermediate	Intermediate	Intermediate	Intermediate	Intermediate	Intermediate	Intermediate	Intermediate	Intermediate	Intermediate	Intermediate
IgRoClaMSys ***	Andesite	Andesite	Andesite	Andesite	Andesite	Andesite	Andesite	Andesite	Andesite	Andesite	Andesite
Major oxides and CIPW norm											
SiO_2	60.48	61.05	60.98	61.55	59.55	59.42	59.49	60.21	60.77	60.44	62.33
TiO_2	0.72	0.68	0.69	0.70	0.75	0.78	0.72	0.73	0.72	0.73	0.68
Al_2O_3	17.18	16.96	17.04	17.04	17.64	17.53	17.74	17.41	17.17	17.35	16.91
$Fe_2O_3^T$	6.14	5.83	5.79	5.79	6.66	6.81	6.52	6.31	5.81	6.24	5.74
MnO	0.12	0.11	0.12	0.11	0.13	0.14	0.12	0.12	0.11	0.12	0.11
MgO	2.38	2.27	2.34	2.38	2.57	2.54	2.6	2.49	2.4	2.48	2.36
CaO	5.84	5.62	5.69	5.64	6.13	6.2	6.06	5.94	5.91	5.93	5.38
Na_2O	3.56	3.64	3.59	3.72	3.58	3.44	3.72	3.65	3.75	3.65	3.69
K_2O	2.38	2.44	2.48	2.44	2.14	2.21	2.08	2.27	2.37	2.28	2.51
P_2O_5	0.15	0.14	0.15	0.13	0.16	0.16	0.15	0.15	0.13	0.14	0.13
LOI	0.59	0.69	0.77	0.44	0.6	0.61	0.58	0.75	0.52	0.56	0.33
Sum	99.54	99.43	99.64	99.94	99.91	99.84	99.78	100.03	99.66	99.92	100.17
$(SiO_2)_{adj}$	61.412	62.108	61.953	62.135	60.272	60.196	60.272	60.942	61.572	61.122	62.705
$(Na_2O + K_2O)_{adj}$	6.032	6.185	6.167	6.219	5.789	5.724	5.876	5.992	6.201	5.997	6.237
Q	13.602	14.273	14.102	14.062	12.192	12.509	11.661	12.712	13.006	12.982	15.116
Or	14.282	14.669	14.890	14.556	12.8000	13.231	12.454	13.578	14.191	13.626	14.922
Ab	30.588	31.335	30.862	31.777	30.66	29.488	31.891	31.261	32.15	31.234	31.411
An	24.235	23.125	23.423	22.805	26.054	26.201	25.899	24.713	23.321	24.496	22.296
Di	3.458	3.557	3.512	3.776	3.030	3.225	2.943	3.401	4.550	3.572	3.048

Hy	9.929	9.339	9.484	9.349	11.107	11.074	11.121	10.364	9.048	10.169	9.599
Mt	2.165	2.059	2.042	2.030	2.341	2.395	2.294	2.218	2.044	2.191	2.005
Il	1.389	1.314	1.331	1.342	1.442	1.501	1.385	1.403	1.386	1.402	1.299
Ap	0.353	0.330	0.353	0.304	0.375	0.376	0.352	0.352	0.305	0.328	0.303
Mg#	50.242	50.354	51.285	51.709	50.130	49.279	50.951	50.689	51.831	50.867	51.714
FeO^T / MgO	2.321	2.311	2.226	2.189	2.332	2.412	2.256	2.280	2.178	2.264	2.189
Trace elements											
Ba	736	742	705	724	689	661	648	712	725	789	779
Co	13	11	14	15	17	16	16	15	10	11	13
Cr	51	60	55	40	58	35	28	39	48	46	47
Cu	12	12	15	11	14	15	15	11	17	13	13
Nb	6.1	4.0	3.8	5.5	4.9	5.9	5.3	4.5	5.5	5.1	5.6
Ni	8	7	8	9	6	8	7	8	5	7	7
Rb	69.2	69.8	59.6	55.5	66.6	49.5	48.8	58.8	52.9	61.8	64
Sr	508.7	503.2	525.5	515.8	522.7	559.9	557.5	522.2	499.5	479.5	477.2
V	98	90	99	108	95	111	118	104	112	97	92
Y	19.4	18.6	18.8	19.9	18.4	19	18.7	18.4	19.3	19.8	19.1
Zn	66	67	75	68	71	76	77	72	69	64	65
Zr	148.2	146.9	139.9	144.4	141.4	138.4	137.4	135.9	142.3	141.4	138.8
Radiogenic isotopes (multiple determinations) ****											
$^{87}Sr/^{86}Sr$	0.704549±18	0.704575±23	0.704571±21	0.704585±13	0.704547±13	0.704508±32	0.704501±23	0.704598±23	0.704523±23	0.704575±20	0.704529±24
	0.704553±13		0.704555±16	0.704566±23	0.704556±16	0.704530±22	0.704515±27	0.704587±24	0.704485±23	0.704560±11	
	0.704545±23		0.704553±12		0.704558±12	0.704485±16	0.704548±13	0.704571±20	0.704466±13		
						0.704513±19		0.704581±11			
$^{143}Nd/^{144}Nd$	0.512729±14	0.512729±20	0.512725±10	0.512733±19	0.512705±13	0.512703±21	0.512707±22	0.512738±19	0.512713±29	0.512703±9	0.512728±34
					0.512733±18	0.512717±28		0.512734±13		0.512697±23	0.512736±11
$^{206}Pb/^{204}Pb$		18.736 (6)		18.746 (7)		18.742 (6)	18.741 (9)				18.737 (7)
$^{207}Pb/^{204}Pb$		15.608 (6)		15.618 (6)		15.621 (5)	15.620 (7)				15.616 (6)
$^{208}Pb/^{204}Pb$		38.532 (12)		38.542 (11)		38.570 (13)	38.577 (16)				38.560 (15)

* “Petrographic type” has the adjective of the most common modal mineral(s).

** The magma and rock types from the IUGS (International Union of Geological Sciences) scheme and CIPW normative minerals were obtained from the IgRoCS computer program (Verma and Rivera-Gómez, 2013).

*** The multidimensional classification scheme consistent with the IUGS scheme involves the use of a series of online computer programs available from the website tlaloc.ier.unam.mx, HMgClaMSys_mlr (Verma et al., 2016b), MagClaMSys_ilr (Verma et al., 2017c), and IgRoClaMSys_ilr (Verma and Rivera-Gómez, 2017); this application constitutes a new test for this classification scheme. The "Common igneous rock" refers to all those igneous rocks that are not identified as any of the High-Mg rocks.

**** The $^{87Sr}/^{86}Sr$ ratios are normalized to $^{86}Sr/^{88}Sr = 0.11940$ and adjusted to SRM987 $^{87}Sr/^{86}Sr$ of 0.710230. The $^{143}Nd/^{144}Nd$ are normalized to $^{146}Nd/^{144}Nd = 0.72190$ and adjusted to La Jolla $^{143}Nd/^{144}Nd$ of 0.511860. The measured $^{87}Sr/^{86}Sr$ for the SRM987 standard was 0.710216 ± 11 (1s; n = 36) and the measured $^{143}Nd/^{144}Nd$ for the La Jolla standard was 0.511833 ± 12 (1s; n = 82). Note the measured isotopic ratios included in Table 1 were adjusted following the convention of Mainz (e.g., Verma, 1992). The analytical uncertainty quoted for Sr and Nd isotope ratios are two times the standard error of the mean ($2s_E$) multiplied by 10^6. The Pb isotope ratios were corrected for fractionation estimated by running simultaneously the NBS-982 standard and are relative to values of $^{206}Pb/^{204}Pb = 36.74432$ and $^{207}Pb/^{206}Pb = 0.46707$ for this standard. All Pb data were corrected for mass fractionation (a factor of 1.48 ± 0.04 (1s; n = 9). For Pb isotope ratios the uncertainties are the combined uncertainties in within-run statistics and in the estimation of fractionation correction, and are multiplied by 10^3.

Table 2
Statistical information on the Nb anomaly (with respect to Ba and La) for intermediate and acid rocks from southern Mexico (this work) and comparison with other arcs and continental rifts (taken from Verma, 2015).

Area	Magma type	$\{Nb/Nb^*\}_{pm}$		$\{Ta/Ta^*\}_{pm}$	
		Mean ± standard deviation (number of samples) $\bar{x}$ ± s (n)	99% Confidence limits or interval of the mean (CL_{99})	Mean ± standard deviation (number of samples) $\bar{x}$ ± s (n)	99% Confidence limits or interval of the mean (CL_{99})
TVC (Tacaná Volcanic Arc)	Basic	––	––	––	––
	Intermediate	0.124 ± 0.016 (29)	0.107 − 0.140	0.144 ± 0.045 (32)	0.100 − 0.189
	Acid	0.112 ± 0.030 (12)	0.083 − 0.142	––	––
CVB (Chiapanecan Volcanic Belt)	Basic	---	––	---	---
	Intermediate	0.222 ± 0.023 (43)	0.199 − 0.244	0.305 ± 0.024 (23)	0.282 − 0.329
	Acid	---	––	---	---
Continental arcs					
Central American Volcanic Arc (front arc)	Basic	0.13 ± 0.06 (59)	0.11 − 0.15	0.18 ± 0.11 (34)	0.13 − 0.23
Central American Volcanic Arc (back arc)	Basic	0.9 ± 0.7 (28)	0.5 − 1.3	0.304 ± 0.038 (6)	0.241 − 0.366
Central American Volcanic Arc	Intermediate	0.108 ± 0.030 (289)	0.103 − 0.113	0.13 ± 0.05 (213)	0.12 − 0.14
	Acid	0.105 ± 0.040 (25)	0.083 − 0.127	0.105 ± 0.029 (4)	0.020 − 0.189
Andes (Chile)	Basic	0.20 ± 0.05 (29)	0.17 − 0.23	0.147 ± 0.037 (9)	0.105 − 0.189
	Intermediate	0.186 ± 0.041 (125)	0.177 − 0.196	0.192 ± 0.043 (65)	0.177 − 0.206
	Acid	0.177 ± 0.031 (49)	0.165 − 0.189	0.194 ± 0.034 (41)	0.180 − 0.208
Andes (Peru)	Acid	0.25 ± 0.10 (37)	0.21 − 0.30	0.26 ± 0.11 (33)	0.21 − 0.31
Andes (Ecuador)	Basic	0.079 ± 0.009 (7)	0.065 − 0.090	––	––
	Intermediate	0.113 ± 0.030 (178)	0.107 − 0.119	0.101 ± 0.044 (44)	0.083 − 0.119
	Acid	0.106 ± 0.018 (210)	0.103 − 0.110	0.17 ± 0.07 (16)	0.11 − 0.22
Andes (Colombia)	Intermediate	0.23 ± 0.05 (11)	0.18 − 0.28	0.23 ± 0.12 (12)	0.12 − 0.34
Continental rifts or extensional areas					
San Luis Potosí (Mexico)	Basic	0.78 ± 0.36 (15)	0.49 − 1.06	1.10 ± 0.44 (4)	––
	Intermediate	0.19 ± 0.05 (4)	0.04 − 0.33	––	––
Baja California (Mexico) − Pliocene−Pleistocene	Basic	0.137 ± 0.012 (4)	0.102 − 0.172	––	––
	Intermediate	0.13 ± 0.05 (32)	0.11 − 0.16	––	––
Baja California (Mexico) − Miocene	Intermediate	0.126 ± 0.022 (15)	0.108 − 0.143	––	––

Mogollon−Datil volcanic field, New Mexico (USA)	Basic	0.75 ± 0.27 (13)	0.52 − 0.98	0.87 ± 0.32 (9)	0.51 − 1.23
	Intermediate	0.163 ± 0.030 (10)	0.133 − 0.194	0.19 ± 0.03 (10)	0.15 − 0.22
Basin and Range, Nevada−Arizona (USA)	Basic	0.62 ± 0.26 (20)	0.45 − 0.78	0.86 ± 0.27 (8)	0.53 − 1.19
	Intermediate	0.22 ± 0.10 (7)	0.08 − 0.35	−−	−−
Rio Grande rift, New Mexico (USA)	Basic	0.7 ± 0.5 (29)	0.5 − 1.0	0.8 ± 0.5 (28)	0.5 − 1.1
	Intermediate	0.21 ± 0.09 (14)	0.13 − 0.28	0.21 ± 0.07 (13)	0.16 − 0.27
San Juan volcanic field, Colorado (USA)	Intermediate	0.17 ± 0.08 (26)	0.13 − 0.22	−−	−−
	Acid	0.12 ± 0.05 (7)	0.06 − 0.19	−−	−−
Western USA	Basic	0.61 ± 0.36 (46)	0.47 − 0.75	0.38 ± 0.06 (14)	0.33 − 0.42
	Intermediate	0.17 ± 0.06 (10)	0.11 − 0.24	−−	−−
Central Mexican Volcanic Belt (near the trench)	Basic	0.54 ± 0.25 (38)	0.43 − 0.65	0.75 ± 0.16 (30)	0.67 − 0.84
Central Mexican Volcanic Belt (far from the trench)	Basic	0.53 ± 0.24 (28)	0.41 − 0.66	−−	−−
Central Mexican Volcanic Belt	Intermediate	0.21 ± 0.09 (498)	0.20 − 0.22	0.25 ± 0.11 (274)	0.23 − 0.27
Central Mexican Volcanic Belt	Acid	0.152 ± 0.033 (194)	0.146 − 0.158	0.22 ± 0.05 (184)	0.21 − 0.23
Northwest Iran	Basic	0.46 ± 0.10 (14)	0.38 − 0.55	0.42 ± 0.08 (8)	0.32 − 0.51
	Intermediate	0.422 ± 0.026 (6)	0.379 − 0.465	−−	−−
Eastern Iran	Basic	0.88 ± 0.11 (6)	0.70 − 1.05	0.90 ± 0.13 (6)	0.68 − 1.12
	Intermediate	0.70 ± 0.33 (7)	0.24 − 1.16	0.8 ± 0.5 (7)	0.1 − 1.4
Eastern Anatolia (Turkey)	Basic	0.782 ± 0.014 (20)	0.773 − 0.791	0.784 ± 0.038 (20)	0.760 − 0.809
	Acid	0.50 ± 0.13 (25)	0.43 − 0.58	0.680 ± 0.017 (24)	0.580 − 0.779
North and Northeast China	Basic	0.78 ± 0.17 (21)	0.67 − 0.88	0.49 ± 0.11 (4)	0.17 − 0.80
	Intermediate	0.47 ± 0.09 (8)	0.36 − 0.57	0.37 ± 0.09 (5)	0.18 − 0.56
NW Africa (Morocco and Mali)	Basic	0.73 ± 0.10 (6)	0.56 − 0.89	0.63 ± 0.15 (5)	0.32 − 0.94
	Intermediate	0.72 ± 0.13 (18)	0.64 − 0.81	0.73 ± 0.13 (10)	0.60 − 0.87

Table 3
Statistical synthesis of geochemical compositional data for intermediate volcanic rocks from the Tacaná Volcanic Complex (TVC), Chiapanecan Volcanic Belt (CVB), and Central American Volcanic Arc (CAVA; data compilation by Verma, 2015); values for n < 5 not reported.

Parameter	TVC				CVB				CAVA front			
	n	X	u_{99}	CL_{99}	n	X	u_{99}	CL_{99}	n	X	u_{99}	CL_{99}
$(SiO_2)_{adj}$	105	60.739	0.306	60.432 - 61.045	78	57.3	0.267	57.033 - 57.567	321	54.126	0.236	53.890 - 54.361
$(TiO_2)_{adj}$	109	0.6621	0.0171	0.6450 - 0.6793	59	0.683	0.0152	0.6678 - 0.6982	292	0.6498	0.0136	0.6362 - 0.6634
$(Al_2O_3)_{adj}$	100	17.556	0.113	17.443 - 17.668	73	18.418	0.165	18.253 - 18.584	390	18.752	0.137	18.615 - 18.888
$(Fe_2O_3^t)_{adj}$	109	6.339	0.175	6.164 - 6.514	90	6.711	0.202	6.509 - 6.913	400	8.426	0.143	8.283 - 8.569
$(MnO)_{adj}$	104	0.11419	0.00193	0.11226 - 0.11612	80	0.17161	0.00403	0.16758 - 0.17565	346	0.15651	0.00214	0.15437 - 0.15864
$(MgO)_{adj}$	87	2.496	0.047	2.449 - 2.543	62	2.274	0.056	2.218 - 2.329	411	3.903	0.139	3.765 - 4.042
$(CaO)_{adj}$	102	6.014	0.076	5.938 - 6.089	90	7.326	0.178	7.148 - 7.504	299	8.812	0.104	8.708 - 8.916
$(Na_2O)_{adj}$	99	3.6908	0.0265	3.6643 - 3.7172	66	4.027	0.053	3.974 - 4.081	411	3.314	0.064	3.250 - 3.379
$(K_2O)_{adj}$	102	2.095	0.050	2.045 - 2.145	75	2.688	0.067	2.620 - 2.755	305	0.7163	0.0381	0.6783 - 0.7544
$(P_2O_5)_{adj}$	100	0.1608	0.0049	0.1559 - 0.1657	78	0.3139	0.0206	0.2933 - 0.3345	327	0.1862	0.0050	0.1811 - 0.1912
La	61	16.805	0.441	16.364 - 17.246	63	29.89	1.22	28.67 - 31.10	309	10.797	0.396	10.401 - 11.193
Ce	59	32.9	0.57	32.33 - 33.47	43	55.59	1.09	54.50 - 56.68	304	22.63	0.70	21.93 - 23.32
Nd	65	16.06	0.70	15.36 - 16.76	41	27.08	0.87	26.21 - 27.96	258	12.959	0.267	12.692 - 13.226
Sm	45	3.297	0.139	3.158 - 3.436	38	5.349	0.240	5.110 - 5.589	221	2.946	0.054	2.892 - 3.001
Eu	39	0.9212	0.0266	0.8946 - 0.9478	28	1.526	0.059	1.468 - 1.585	238	1.0164	0.0149	1.0016 - 1.0313
Tb	48	0.4652	0.0290	0.4362 - 0.4942	34	0.7056	0.0275	0.6781 - 0.7331	183	0.4427	0.0073	0.4354 - 0.4500
Yb	47	1.557	0.065	1.492 - 1.622	42	2.092	0.083	2.009 - 2.174	200	1.5292	0.0284	1.5007 - 1.5576
Lu	47	0.2349	0.0094	0.2255 - 0.2442	33	0.3188	0.0166	0.3021 - 0.3354	152	0.22713	0.00383	0.22330 - 0.23096
Ba	100	713.2	10.4	702.9 - 723.6	62	746.6	15.3	731.3 - 761.9	322	537.2	18.2	519.1 - 555.4
Co	75	14.29	0.59	13.70 - 14.89	45	11.76	0.82	10.93 - 12.58	113	23.56	0.70	22.86 - 24.25
Cr	63	8.94	1.65	7.28 - 10.59	64	12.74	2.06	10.68 - 14.80	203	17.79	2.67	15.12 - 20.46
Cs	43	2.193	0.144	2.049 - 2.337	27	2.861	0.439	2.421 - 3.300	197	0.2482	0.0123	0.2359 - 0.2605
Cu	74	12.74	1.10	11.64 - 13.84	82	25.06	3.89	21.17 - 28.95	179	74.5	7.8	66.7 - 82.3
Hf	44	3.823	0.134	3.689 - 3.956	31	3.315	0.285	3.030 - 3.601	151	1.478	0.058	1.420 - 1.536
Nb	49	4.922	0.318	4.604 - 5.241	60	11.79	0.96	10.83 - 12.75	194	3.540	0.110	3.430 - 3.650
Ni	52	8.12	0.81	7.31 - 8.92	59	7.32	1.10	6.22 - 8.42	272	19.926	2.11	17.816 - 22.037
Pb	59	11.51	0.71	10.80 - 12.23	66	7.71	0.68	7.03 - 8.40	170	3.298	0.150	3.147 - 3.448
Rb	112	53.34	2.60	50.74 - 55.94	68	76.62	3.01	73.61 - 79.63	240	11.02	0.52	10.50 - 11.55

Sb	20	0.6350	0.0313	0.6037 - 0.6663	13	0.249	0.058	0.191 - 0.308	7	0.271	0.280	-0.009 - 0.552
Sc	43	11.59	0.51	11.08 - 12.10	55	10	0.72	9.28 - 10.72	278	21.16	0.77	20.39 - 21.93
Sr	100	518.1	7.8	510.3 - 525.8	59	996.3	33.4	962.9 - 1029.8	227	666.2	10.1	656.0 - 676.3
Ta	36	0.374	0.135	0.239 - 0.510	22	0.93	0.063	0.866 - 0.993	166	0.2516	0.0159	0.2358 - 0.2675
Th	64	3.724	0.194	3.530 - 3.918	72	7.52	0.57	6.95 - 8.09	250	0.968	0.052	0.915 - 1.020
U	38	1.312	0.073	1.239 - 1.386	31	2.727	0.206	2.522 - 2.933	226	0.3669	0.0181	0.3488 - 0.3850
V	83	107.65	3.04	104.61 - 110.69	64	166.6	6.4	160.2 – 173.0	198	163.5	8.7	154.8 - 172.2
Y	99	16.01	0.59	15.42 - 16.60	77	22.35	1.03	21.31 - 23.38	240	16.383	0.389	15.994 - 16.772
Zn	93	76.51	2.39	74.12 - 78.90	78	69.28	3.09	66.20 - 72.37	138	80.89	2.25	78.63 - 83.14
Zr	111	138.86	4.11	134.75 - 142.98	68	164.5	8.3	156.2 - 172.8	242	56.65	2.79	53.86 - 59.43
$(LILE4/LREE3)_E$	61	3.752	0.126	3.626 - 3.878	39	2.681	0.107	2.574 - 2.789	211	2.6755	0.0326	2.6429 - 2.7081
$(LILE5/HFSE5a)_E$	37	8.23	0.85	7.38 - 9.09	14	5.658	0.353	5.305 - 6.012	94	5.843	0.089	5.754 - 5.932
$(LILE4/HFSE4a)_E$	45	7.975	0.322	7.653 - 8.297	14	5.901	0.303	5.598 - 6.204	191	6.542	0.227	6.315 - 6.769
$(LILE4/HFSE4b)_E$	37	8.45	1.07	7.38 - 9.52	18	5.247	0.288	4.959 - 5.535	159	6.276	0.179	6.097 - 6.454
$(LILE4/HFSE4c)_E$	64	8.829	0.431	8.398 - 9.260	50	6.102	0.409	5.693 - 6.511	257	6.641	0.225	6.416 - 6.866
$(LILE4/HFSE3a)_E$	111	9.129	0.283	8.847 - 9.412	68	7.59	0.49	7.10 - 8.08	312	6.409	0.177	6.232 - 6.585
$(LREE3/HFSE5a)_E$	37	2.114	0.153	1.962 - 2.267	15	1.903	0.085	1.818 - 1.988	128	2.379	0.057	2.322 - 2.436
$(LREE3/HFSE4a)_E$	47	2.135	0.056	2.079 - 2.190	24	2.550	0.262	2.287 - 2.812	192	2.198	0.109	2.089 - 2.307

Table 4
Statistical synthesis of geochemical compositional data for lithic fragments or enclaves of intermediate compositions from the Tacaná Volcanic Complex (TVC) and Chiapanecan Volcanic Belt (CVB); values for n < 5 not reported.

Parameter	TVC				CVB			
	n	X	u_{99}	CL_{99}	n	X	u_{99}	CL_{99}
$(SiO_2)_{adj}$	24	58.78	2.23	56.55 - 61.01	13	61.34	1.10	60.24 - 62.44
$(TiO_2)_{adj}$	24	0.723	0.092	0.631 - 0.816	15	0.555	0.075	0.480 - 0.630
$(Al_2O_3)_{adj}$	22	17.835	0.401	17.434 - 18.237	15	18.22	0.52	17.69 - 18.74
$(Fe_2O_3^t)_{adj}$	24	6.86	0.84	6.02 - 7.69	15	5.62	0.58	5.03 - 6.20
$(MnO)_{adj}$	24	0.1222	0.0087	0.1135 - 0.1310	15	0.1453	0.0226	0.1227 - 0.1679
$(MgO)_{adj}$	21	2.57	0.53	2.04 - 3.10	13	1.467	0.17	1.297 - 1.636
$(CaO)_{adj}$	21	6.46	0.68	5.78 - 7.14	13	6.074	0.342	5.731 - 6.416
$(Na_2O)_{adj}$	23	3.629	0.107	3.522 - 3.735	15	4.163	0.182	3.981 - 4.345
$(K_2O)_{adj}$	24	1.817	0.289	1.528 - 2.106	13	2.648	0.283	2.365 - 2.931
$(P_2O_5)_{adj}$	20	0.1557	0.0098	0.1459 - 0.1656	15	0.249	0.046	0.203 - 0.294
La	18	14.35	2.071	12.279 - 16.421	9	28.5	8.5	20.0 - 37.0
Ce	18	30.406	3.242	27.163 - 33.648	9	50.9	12.8	38.1 - 63.7
Nd	17	14.20	1.08	13.12 - 15.28	9	24.2	6.5	17.7 - 30.7
Sm	14	3.091	0.155	2.936 - 3.247	8	4.54	1.18	3.360 - 5.720
Eu	14	0.8856	0.0263	0.8593 - 0.9119	8	1.289	0.153	1.135 - 1.442
Tb	14	0.462	0.059	0.403 - 0.522	8	0.725	0.322	0.403 - 1.047
Yb	14	1.576	0.122	1.454 - 1.698	8	2.10	0.70	1.40 - 2.79
Lu	14	0.2372	0.0165	0.2207 - 0.2537	8	0.299	0.106	0.193 - 0.405
Ba	24	641	75	566 - 716	15	708	56	652 - 765
Co	13	15.58	2.76	12.81 - 18.34	14	20.1	9.2	10.9 - 29.3
Cr	18	19.9	8.9	10.9 - 28.8	12	9.70	3.76	5.94 - 13.46
Cs	14	2.007	0.355	1.652 - 2.362	6	3.53	1.34	2.20 - 4.87
Cu	9	20.9	18.6	2.3 - 39.5	15	23.53	11.8	11.73 - 35.34
Hf	12	3.558	0.334	3.224 - 3.893	6	3.78	1.08	2.70 - 4.86
Nb	7	3.77	1.14	2.63 - 4.91	14	20	6.7	10.3 - 23.7
Rb	24	46.4	9.2	37.2 - 55.6	14	84.9	9.4	75.5 - 94.4
Sc	14	12.96	3.62	9.35 - 16.57	7	7.85	2.74	5.110 - 10.590
Sr	21	508.1	22.2	485.8 - 530.3	15	723	105	617 - 828
Th	15	3.25	0.58	2.66 - 3.83	15	7.46	1.64	5.82 - 9.10
U	14	1.101	0.240	0.860 - 1.341	6	3.70	1.11	2.59 - 4.81
V	19	130.4	24.6	105.8 - 155.0	15	110.7	26.9	83.7 - 137.6
Y	24	16.78	1.05	15.73 - 17.82	15	25.07	3.99	21.08 - 29.06
Zn	11	77.8	11.2	66.7 - 89.0	15	60.0	8.0	56.0 - 72.0
Zr	24	133.1	18.3	114.8 - 151.4	14	173.8	32.3	141.5 - 206.1
$(LILE4/LREE3)_E$	17	3.895	0.216	3.679 - 4.111	8	3.06	0.57	2.49 - 3.63
$(LILE4/HFSE4a)_E$	14	8.16	0.8	7.36 - 8.96	6	9	0.99	8.01 - 9.99
$(LILE4/HFSE4c)_E$	8	6.88	2.31	4.57 - 9.20	13	6.59	0.96	5.63 - 7.55
$(LILE4/HFSE3a)_E$	24	8.28	1.25	7.03 - 9.53	14	9.09	0.96	8.14 - 10.05
$(LREE3/HFSE4a)_E$	14	2.081	0.125	1.956 - 2.206	6	3.14	0.51	2.63 - 3.64

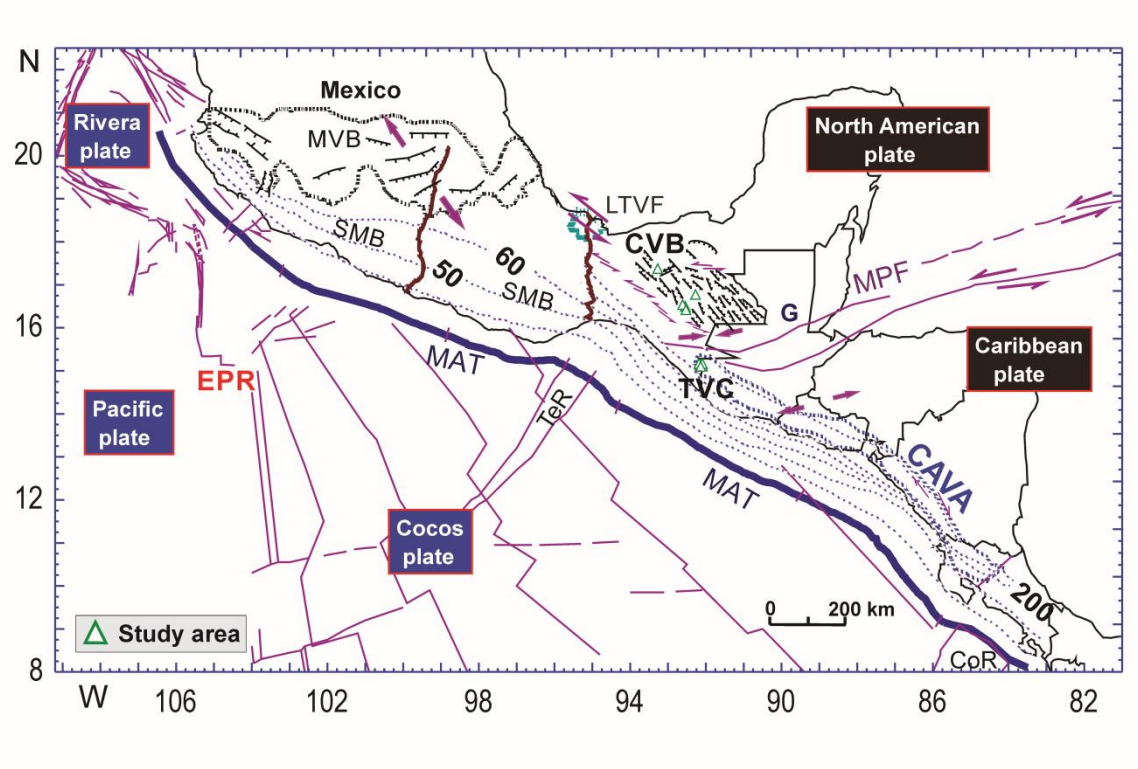

Figure 1

Fig. 1.

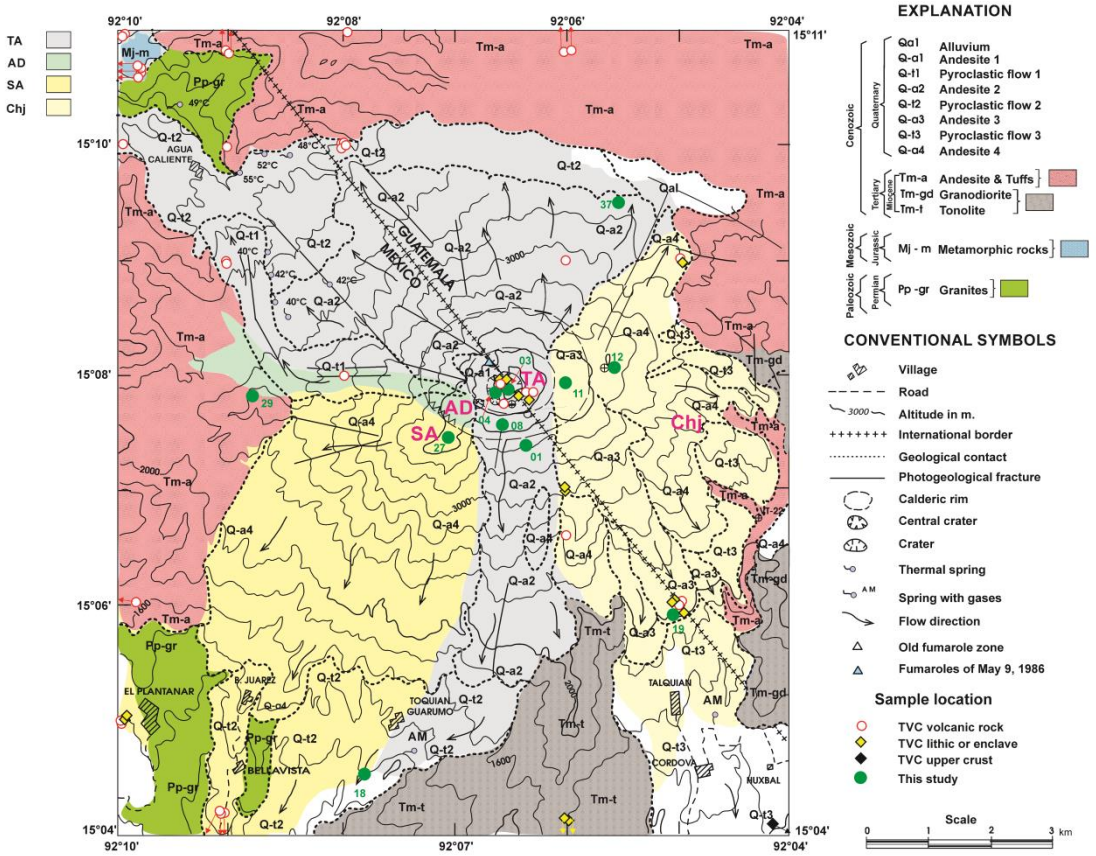

Figure 2

Fig. 2.

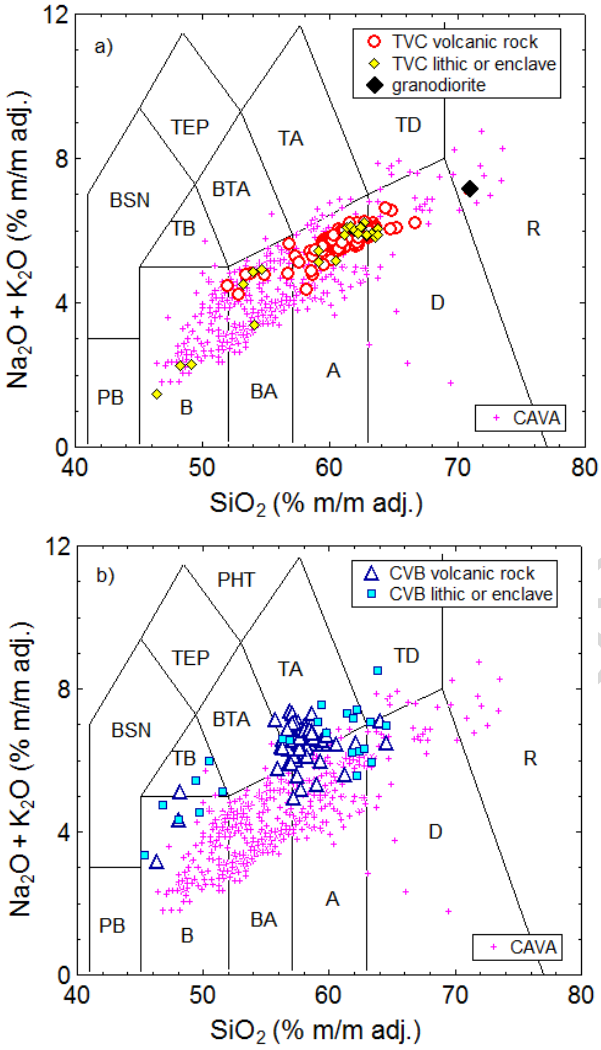

Fig. 3.

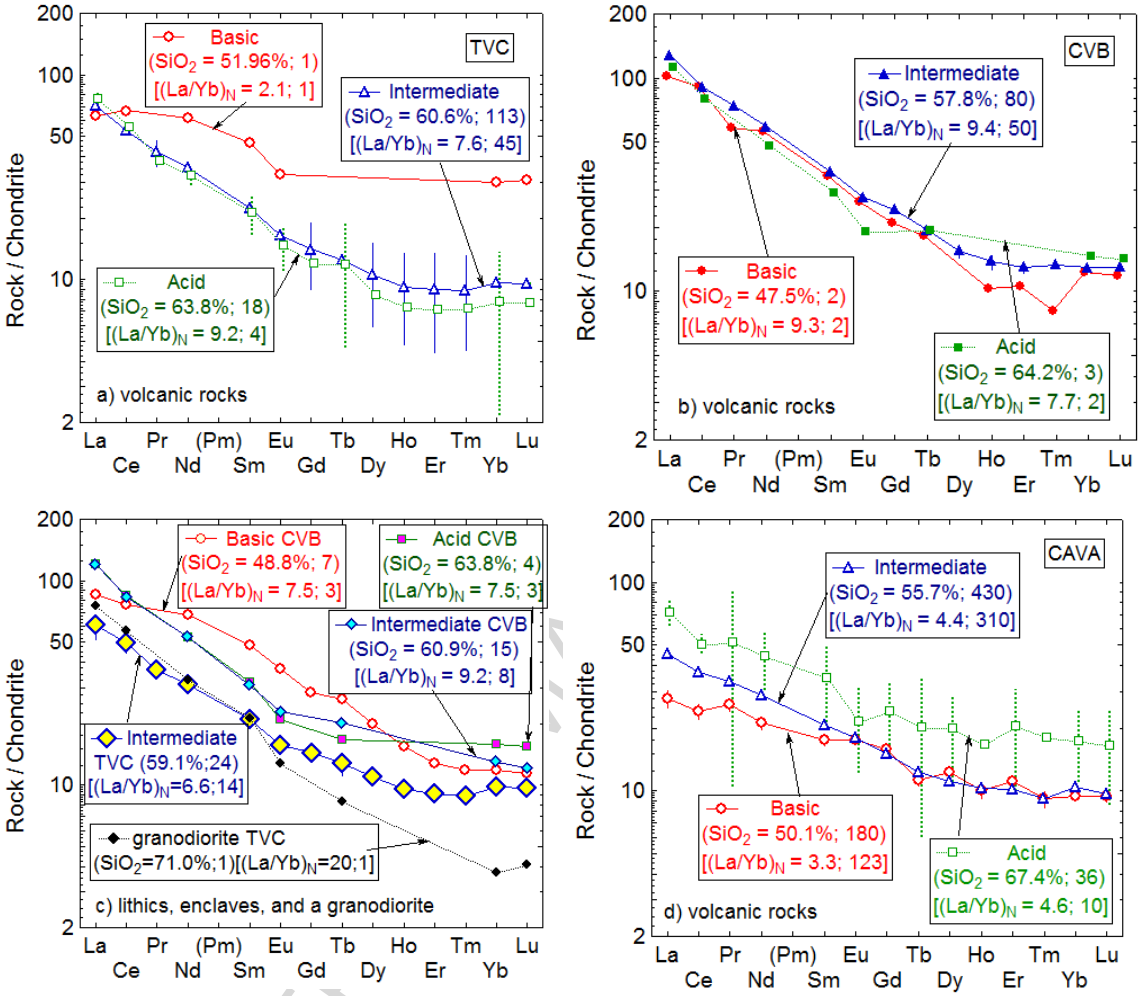

Fig. 4.

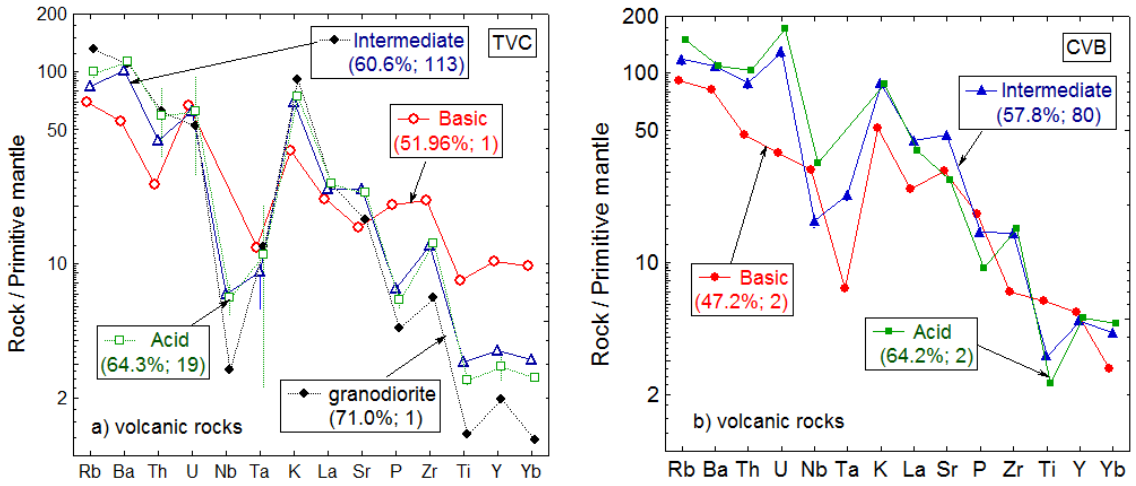

Fig. 5.

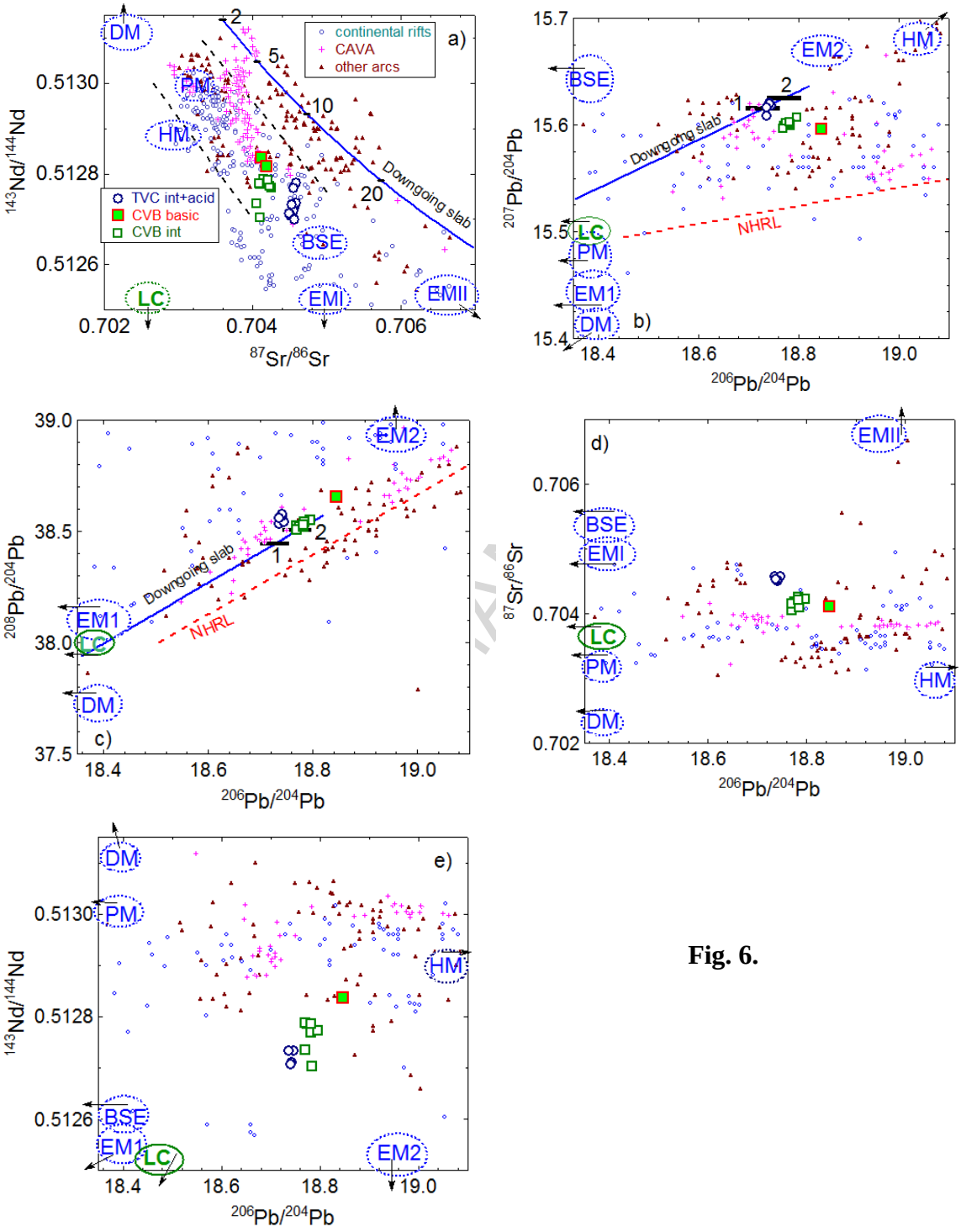

Fig. 6.

H i g h t l i g h t s

New geochemical and radiogenic isotope data for the Volcán Tacaná

The first paper with statistical treatment of all geochemical data of southern Mexican rocks

The first statistical comparison of two volcanic provinces in southern Mexico

Use of combined subduction-sensitive parameters in southern Mexico